

¹ **Whole-brain comparison of rodent and human brains
using spatial transcriptomics**

³

⁴ Antoine Beauchamp^{1,2,3,*}, Yohan Yee^{1,2,3}, Ben C. Darwin^{1,2}, Armin Raznahan⁴, Rogier B.
⁵ Mars^{5,6,†}, Jason P. Lerch^{1,2,3,5,*†}

⁶

⁷ ¹Mouse Imaging Centre, Toronto, Ontario, Canada.

⁸ ²The Hospital for Sick Children, Toronto, Ontario, Canada.

⁹ ³Department of Medical Biophysics, University of Toronto, Toronto, Ontario, Canada.

¹⁰ ⁴Section on Developmental Neurogenomics, Human Genetics Branch, National Institute of Mental Health Intramural
¹¹ Research Program, Bethesda, MD, U.S.A.

¹² ⁵Wellcome Centre for Integrative Neuroimaging, Centre for Functional MRI of the Brain (FMRIB), Nuffield Depart-
¹³ ment of Clinical Neurosciences, John Radcliffe Hospital, University of Oxford, Oxford, United Kingdom.

¹⁴ ⁶Donders Institute for Brain, Cognition and Behaviour, Radboud University Nijmegen, Nijmegen, Netherlands.

¹⁵ [†]These authors contributed equally to this work.

¹⁶ *Corresponding author. Email: antoine.beauchamp@mail.utoronto.ca (A.B.); jason.lerch@ndcn.ox.ac.uk (J.P.L)

¹⁷ **Abstract**

¹⁸ The ever-increasing use of mouse models in preclinical neuroscience research calls for an improvement in the
¹⁹ methods used to translate findings between mouse and human brains. Previously we showed that the brains
²⁰ of primates can be compared in a direct quantitative manner using a common reference space built from
²¹ white matter tractography data (Rogier B. Mars et al., 2018b). Here we extend the common space approach
²² to evaluate the similarity of mouse and human brain regions using openly accessible brain-wide transcrip-
²³ tomic data sets. We show that mouse-human homologous genes capture broad patterns of neuroanatomical
²⁴ organization, but that the resolution of cross-species correspondences can be improved using a novel su-
²⁵ pervised machine learning approach. Using this method, we demonstrate that sensorimotor subdivisions of
²⁶ the neocortex exhibit greater similarity between species, compared with supramodal subdivisions, and that
²⁷ mouse isocortical regions separate into sensorimotor and supramodal clusters based on their similarity to
²⁸ human cortical regions. We also find that mouse and human striatal regions are strongly conserved, with
²⁹ the mouse caudoputamen exhibiting an equal degree of similarity to both the human caudate and putamen.

30 Introduction

31 Animal models play an indispensable role in neuroscience research, not only for understanding disease and
32 developing treatments, but also for obtaining data that cannot be obtained in the human. While numerous
33 species have been used to model the human brain, the mouse has emerged as the most prominent of these,
34 due to its rapid life cycle, straightforward husbandry, and amenability to genetic engineering (Dietrich et
35 al., 2014; Ellenbroek and Youn, 2016; Hedrich et al., 2004; Houdebine, 2004). Mouse models have proven
36 to be extremely useful for understanding diverse features of the brain, from its molecular neurobiological
37 properties to its large-scale network properties (Hodge et al., 2019; Oh et al., 2014; Yao et al., 2021).
38 However, translating findings from the mouse to the human has not been straightforward. This is especially
39 evident in the context of neuropsychopharmacology, where promising neuropsychiatric drugs have one of the
40 highest failures rates in Phase III clinical trials (Hay et al., 2014).

41 Successful translation requires an understanding of how effects on the brain of the model species are likely to
42 manifest in the brain of the actual species of interest. This is not trivial in the case of the mouse and human,
43 as the two species diverged from a common ancestor about 80 million years ago (Kaas, 2012). Although
44 common themes are apparent in the brains of all mammalian species studied to date (Krubitzer, 2007), there
45 remain substantial differences between the mouse and human brain. Beyond the obvious differences in size,
46 large parts of the human cortex potentially have no corresponding homologues in the mouse (Preuss, 1995).
47 Direct comparisons across the brains of different species are further complicated by the fact that researchers
48 from different traditions use inconsistent nomenclature to refer to similar neuroanatomical areas (Heukelum
49 et al., 2020; Laubach et al., 2018).

50 Over the course of the last decade, we have developed novel approaches to explicitly evaluate similarities
51 and differences between the brains of related species. These approaches describe brains using common data
52 spaces that are directly comparable between species, making it possible to evaluate the similarity of different
53 regions in a quantitative fashion (Mars et al., 2021). This way, potential homologues can be formally tested
54 and regions of the brain that do not allow for straightforward translation can be identified (Rogier B. Mars
55 et al., 2018b). Establishing such a formal translation between the mouse and the human brain would allow
56 scientists involved in translational research to explicitly test hypotheses about conservation of brain regions,
57 identify regions that are well suited to translational paradigms, and directly transform quantitative maps
58 from the brain of one species to the other.

59 One approach towards building these common spaces has been to exploit connectivity. It has previously
60 been demonstrated that brain regions can be identified via their unique set of connections to other regions

61 in the brain. This *connectivity fingerprint* can therefore be seen as a diagnostic of an area (Rogier B. Mars
62 et al., 2018a; Passingham et al., 2002). The common connectivity space approach relies on defining agreed
63 upon neuroanatomical homologues *a priori* and then expressing the connectivity fingerprint of regions under
64 investigation with those established homologues in the two brains (Mars et al., 2016b). The connections
65 of any given region to the established homologues thus form a common space, which links the two brains.
66 In a series of early studies, we compared the connectivity of the macaque and human brain, identifying
67 homologies as well as specializations across association cortex (Mars et al., 2013; Neubert et al., 2014; Sallet
68 et al., 2013). The same approach has recently been applied to mouse-human comparisons for the first time,
69 demonstrating conserved organization between the mouse and human striatum, but some specialization in
70 the human caudate related to connectivity with the prefrontal cortex (Balsters et al., 2020). A similar study
71 recently compared connectivity of the medial frontal cortex across rats, marmosets, and humans (Schaeffer et
72 al., 2020). However, the lack of established neuroanatomical homologues in mice, particularly in the cortex,
73 limits the use of connectivity to compare these species.

74 A more promising approach to mouse-human comparisons could be to exploit the spatial patterns of gene
75 expression. Advances in transcriptomic mapping can be used to characterise the differential expression of
76 many thousands of genes across the brain and compare the pattern between regions (Ortiz et al., 2020).
77 Moreover, the availability of whole-brain spatial transcriptomic data sets for multiple species provides an
78 opportunity to run novel analyses at low cost (Hawrylycz et al., 2012; Lein et al., 2007). Such maps for the
79 human cortex show topographic patterns that mimic those observed in other modalities, such as a gradient
80 between primary and heteromodal areas of the neocortex (Burt et al., 2018). Importantly, these patterns
81 appear to be conserved across mammalian species (Fulcher et al., 2019), which opens up the possibility
82 of using the expression of homologous genes as a common space across species. In fact, a recent study
83 demonstrated how the expression of homologous genes can be used to directly register mouse and vole brains
84 into a common reference frame, which allows for direct point-xby-point comparisons of brain maps (Englund
85 et al., 2021). However, this specific approach is only feasible because of the large degree of morphological
86 similarity between mouse and vole brains. In the case of mouse-human comparisons, we almost certainly
87 cannot directly register mouse and human brains into a common coordinate frame using methods for image
88 registration. Hence we need to be more creative in our approach.

89 Here we examine the patterns of similarity between the mouse and human brain using a common space
90 constructed from spatial gene expression data sets. We begin with an initial set of 2835 homologous genes.
91 Subsequently, we present and evaluate a novel method for improving the resolution of mouse-human neu-
92 roanatomical correspondences using a supervised machine learning approach. Using the novel representation

93 of the gene expression common space, i.e. a latent gene expression space, we analyse the similarity of mouse
94 and human isocortical subdivisions and demonstrate that sensorimotor regions exhibit a higher degree of sim-
95 ilarity than supramodal regions. Finally, we examine the patterns of transcriptomic similarity at a voxel-wise
96 level in the mouse and human striatum.

97 Results

98 Homologous genes capture broad similarities in the mouse and human brains

99 We first examined the pattern of similarities that emerged when comparing mouse and human brain regions
100 on the basis of their gene expression profiles. We constructed a gene expression common space using widely
101 available data sets from the Allen Institute for Brain Science: the Allen Mouse Brain Atlas (AMBA) and
102 the Allen Human Brain Atlas (AHBA) (Hawrylycz et al., 2012; Lein et al., 2007). These data sets provide
103 whole-brain coverage of expression intensity for thousands of genes in the mouse and human genomes. For
104 our purposes we filtered these gene sets to retain only mouse-human homologous genes using a list of ortho-
105 logues obtained from the NCBI HomoloGene system (NCBI 2018). Using a gene enrichment analysis, we
106 found that this reduced gene set was significantly associated with a number of biological processes related to
107 the nervous system, with Gene Ontology labels such as “nervous system development”, “neurogenesis”, and
108 “regulation of nervous system development”. Additional modules returned with high significance were “reg-
109 ulation of multicellular organismal process”, “regulation of biological quality”, and “multicellular organism
110 development”. The full set of significant modules can be found in Supplementary File 1.

111 Prior to analysis, the mouse and human homologous gene expression data sets were pre-processed using a
112 pipeline that included quality control checks, normalization procedures, and aggregation of the expression
113 values under a set of atlas labels. The result was a gene-by-region matrix in either species, describing the
114 normalized expression of 2835 homologous genes across 67 mouse regions and 88 human regions (see Materials
115 and methods). We quantified the degree of similarity between all pairs of mouse and human regions using
116 the Pearson correlation coefficient, resulting in a mouse-human similarity matrix (Figure 1A).

117 We find that the similarity matrix exhibits broad patterns of positive correlation between the mouse and
118 human brains. These clusters of similarity correspond to coarse neuroanatomical regions that are generally
119 well-defined in both species. For instance, we observe that, overall, the mouse isocortex is similar to the
120 human cerebral cortex, with the exception of the hippocampal formation, which forms a unique cluster.
121 Similarly the mouse and human cerebellar hemispheres cluster together, while the cerebellar nuclei show

122 relatively high correlation to each other ($r = 0.404$) as well as to brain stem structures like the pons ($r = 0.359$
123 and $r = 0.371$ for the mouse and human nuclei respectively) and myelencephalon ($r = 0.318$ and $r = 0.374$).
124 The associations between broad regions such as these are self-evident in the correlation matrix.

125 Our ability to resolve regional matches on a finer scale is limited when using all homologous genes in this way.
126 This is especially true for regions within the cerebral and cerebellar cortices, which exhibit a high degree
127 of internal homogeneity. This is apparent in the similarity profiles, defined here as the set of correlation
128 values between a given seed region and all target regions in the other species. For example, the human
129 precentral gyrus and cuneus are most strongly correlated to many regions of the mouse isocortex. While
130 the brain maps feature a rostral-caudal gradient (Figure 1B), the profiles of the two seeds are highly similar
131 despite the regions having very different functions (Figure 1C). Indeed, the correlation between the similarity
132 profiles of the precentral gyrus and cuneus is $r = 0.980$. The similarity profile of human cerebellar crus 1
133 highlights another example of this homogeneity. The profile of crus 1 is similar to that of all regions of the
134 mouse cerebellum, with an average correlation of $r = 0.269$ and a standard deviation of $\sigma = 0.041$. Across
135 all regions, the variance of the correlations across cortical regions is $\sigma^2 = 0.0052$ while that across cerebellar
136 hemispheric regions is $\sigma^2 = 0.0017$, compared with a total variation of $\sigma^2 = 0.0416$ across all entries in the
137 matrix.

138 So, although there is some distinguishing power in the profiles of regions at a finer scale, this is much smaller
139 than between coarse anatomical regions. This is also true for parts of the broad anatomical systems that are
140 part of the same functional system. This suggests that the regional expression patterns of mouse-human
141 homologous genes can be used to identify general similarities between the brains of the two species even
142 using a simple correlation measure, but the ability to identify finer scale matches might require a more
143 subtle approach.

144 **A latent gene expression space improves the resolution of mouse-human associations**
145

146 In the previous analyses, we showed that the expression profiles of homologous genes capture broad simi-
147 larities across the mouse and the human for the major subdivisions of the brain. Some information at a
148 finer resolution (e.g. within the isocortex) was also evident, but much less distinctive. Our next goal was
149 to investigate whether it is possible to leverage the gene expression data sets to relate mouse and human
150 brains to one another at a finer regional level. In order to do so, we sought to maximise the informational
151 value in the set of 2835 homologous genes by creating a new latent common space that exploits the regional

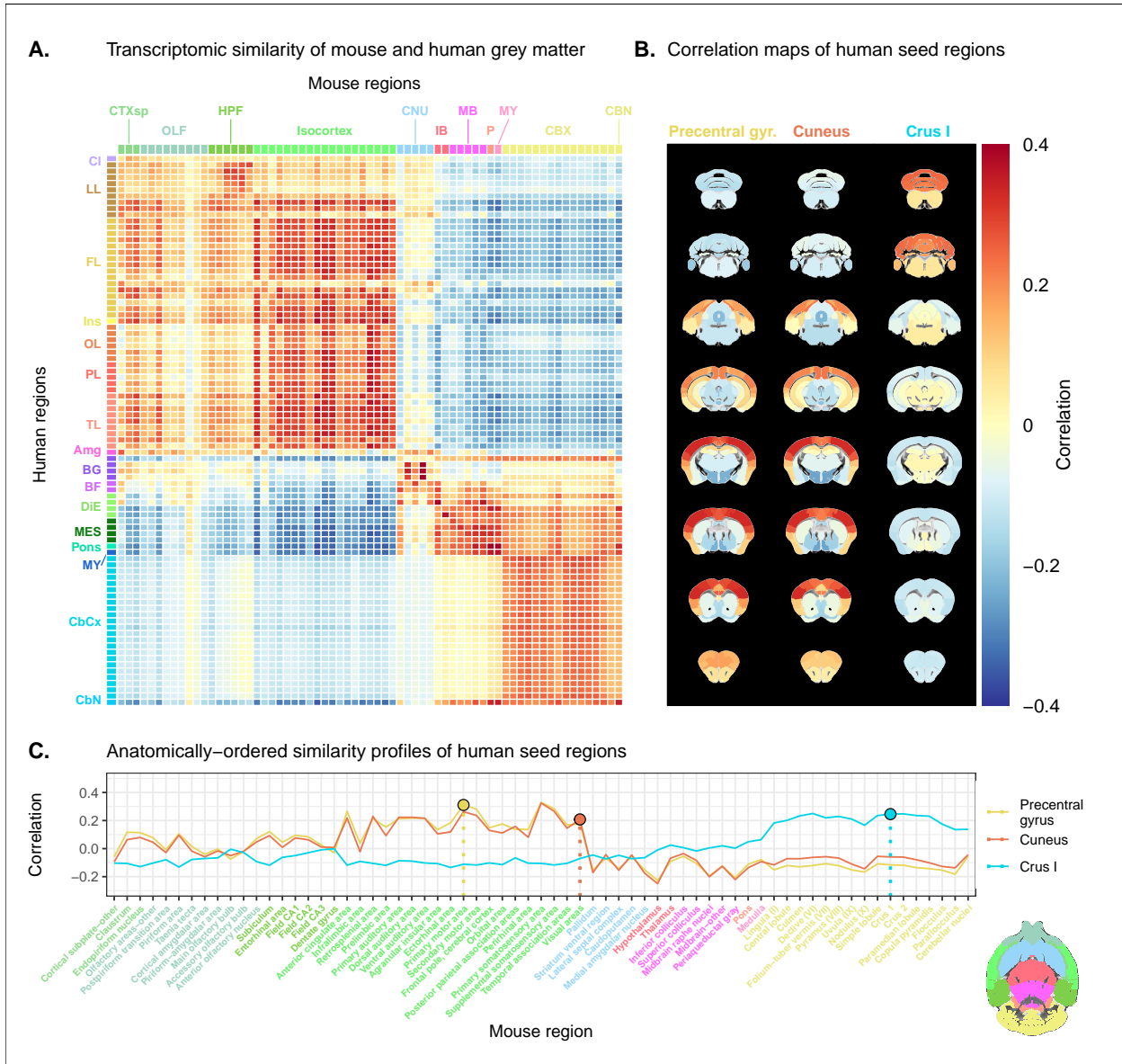


Figure 1. Transcriptomic similarity in the mouse and human brains. **(A)** Similarity matrix displaying the correlation between 67 mouse regions and 88 human regions based on the expression of 2835 homologous genes. Columns are annotated with 11 broad mouse regions: Cortical subplate (CTXsp), olfactory areas (OLF), hippocampal formation (HPF), isocortex, cerebral nuclei (CNU), interbrain (IB), midbrain (MB), pons (P), medulla (MY), cerebellar cortex (CBX), cerebellar nuclei (CBN). Rows are annotated with 16 broad human regions: Claustrum (Cl), limbic lobe (LL), frontal lobe (FL), insula (Ins), occipital lobe (OL), parietal lobe (PL), temporal lobe (TL), amygdala (Amg), basal ganglia (BG), basal forebrain (BF), diencephalon (DIE), mesencephalon (MES), pons, myelencephalon (MY), cerebellar cortex (CbCx), cerebellar nuclei (CbN). Broad patterns of similarity are evident between coarsely defined brain regions, while correlation patterns are mostly homogeneous within these regions. **(B)** Mouse brain coronal slices showing similarity profiles for the human precentral gyrus, cuneus and crus I. Correlation patterns for the precentral gyrus and cuneus are highly similar to one another and broadly similar to most isocortical regions. The crus I is homogeneously similar to the mouse cerebellum. **(C)** Anatomically-ordered line charts displaying the similarity profiles for the seed regions in (B). Dashed vertical lines indicate the canonical mouse homologue for each human seed. Annotation colours correspond to atlas colours from the AMBA and AHBA for mouse and human regions respectively.

152 distinctiveness of the expression profiles.

153 The approach used in the previous analysis relied on using homologous genes as a common space between
154 the mouse and human brain. This approach effectively assigns equal value to each gene, whereas a more
155 powerful approach would be to weight genes by their ability to distinguish between different brain regions.
156 We investigated whether we could accomplish this by constructing a new set of variables from combinations
157 of the homologous genes. Our primary goal here was to transform the initial gene space into a new common
158 space that would improve the locality of the matches. However while we sought a transformation that would
159 allow us to recapitulate known mouse-human neuroanatomical homologues, we also wanted to avoid directly
160 encoding such correspondences in the transformation. Using this information as part of the optimization
161 process for the transformation would run the risk of driving the transformation towards mouse-human pairs
162 that are already known. While we are interested in being able to recover such matches, we are equally
163 interested in identifying novel and unexpected associations between neuroanatomical regions in the mouse
164 and human brains (e.g. one-to-many correspondences). Given these criteria, our approach to identifying an
165 appropriate transformation was to train a multi-layer perceptron classifier on the data from the AMBA. The
166 classifier was tasked with predicting the 67 labels in our mouse atlas from the voxel-wise expression of the
167 homologous genes (Figure 2A).

168 While the model could have been trained using the data from either species, we chose to use the mouse
169 data because it provides continuous coverage of the entire brain and is thus better suited to this purpose.
170 In training the model to perform this classification task, we effectively optimize the network architecture
171 to identify a transformation from the input gene space to a space that encodes information about the
172 delineation between mouse brain regions. To extract this transformation, we removed the output layer from
173 the trained neural network. The resulting architecture defines a transformation from the input space to
174 a lower-dimensional gene expression latent space. We then applied this transformation to the mouse and
175 human gene-by-region expression matrices to obtain representations of the data in the latent common space
176 (Figure 2B). Finally, we used these gene expression latent common space matrices to compute the new
177 similarity matrix (Figure 2C). Since the optimization algorithm used to train the perceptron features an
178 inherent degree of stochasticity, we repeated this training and transformation process 500 times to generate
179 a distribution of latent spaces and similarity matrices over training runs. Although the neural network and
180 associated latent space do not directly provide information about which genes are most important for the
181 classification of specific mouse atlas labels, this type of information can be derived from the model using
182 attribution methods such as integrated gradients (Figure 2-figure supplement 1) (Sundararajan et al., 2017).
183 Each brain region in the classification task is associated with the input genes in different ways, such that

184 there isn't a single weighting of gene importance for the entire model. While most genes contribute to the
 185 classification of any given label in some capacity, it is often the case that the network relies on a reduced
 186 subset of genes to arrive at a decision. For example, the genes *Prrg2* and *Rgs2* were found to be most
 187 influential for the classification of the caudoputamen, when the feature attributions were averaged over all
 188 training runs. In contrast, *Rfx4* and *Tnncl* were the most influential for the classification of the primary
 189 motor area. In some cases, the spatial expression pattern of the gene clearly shows a demarcation of the
 190 region of interest (e.g. *Rgs2*), but this is not always the case, nor is it necessary, as the network learns from
 191 the entire gene expression signature of all voxels.

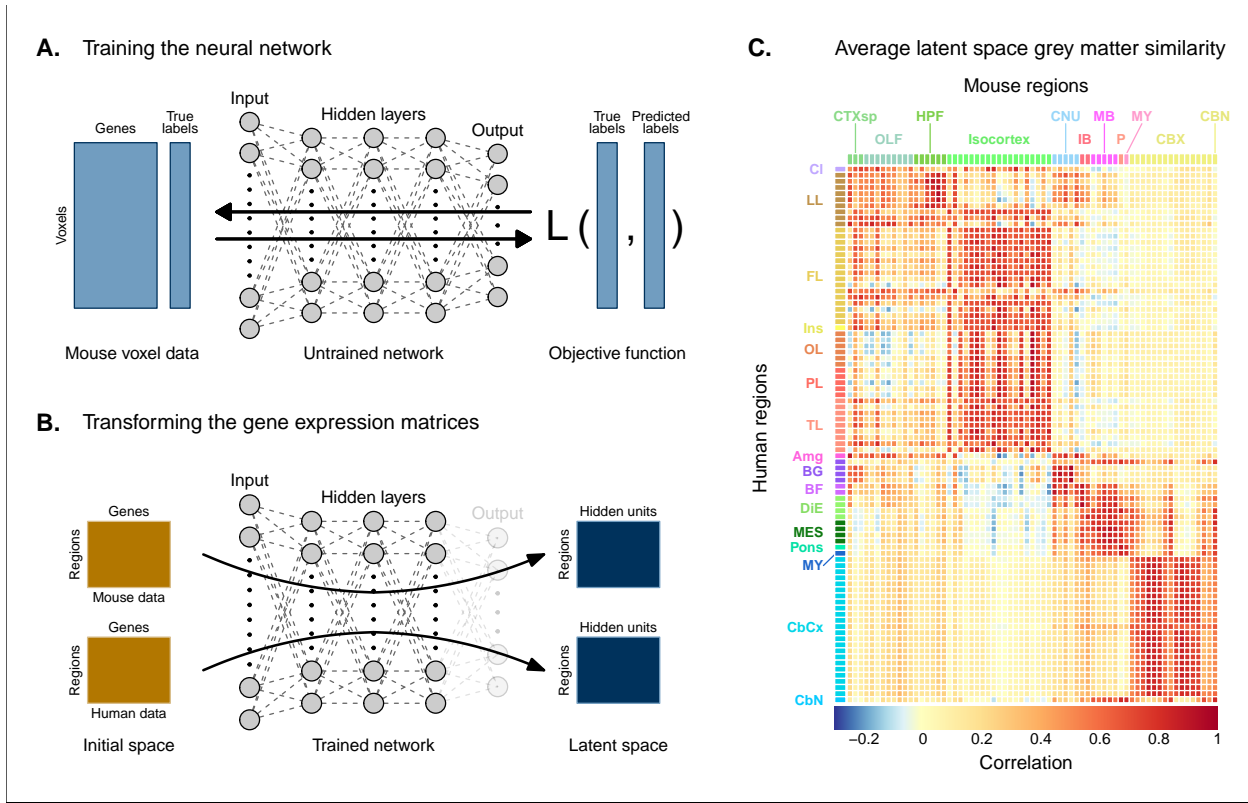


Figure 2. Creating a new common space. **(A)** Voxel-wise expression maps from 2835 homologous genes in the AMBA were used to train the neural network to classify each mouse voxel into one of 67 atlas regions. **(B)** Once the network is trained, the output layer is removed. The mouse and human regional gene expression matrices are passed through the network, resulting in lower-dimensional latent space representations of the data. The training and transformation process was repeated 500 times. **(C)** A similarity matrix displaying the gene expression latent space correlation between mouse and human regions, averaged over 500 neural network training runs. Similar brain regions exhibit very high correlation values. Column and row annotations as described in Figure 1.

192 To assess whether the latent space representations of the data improved the resolution of the mouse-human
 193 matches, we considered two criteria. The first was whether the similarity profiles of the mouse atlas regions
 194 were more localized within the corresponding broad regions of interest (e.g. primary motor area within
 195 isocortex), compared with their similarity profiles in the original gene space. We term this the locality
 196 criterion. The second criterion was whether the degree of similarity between canonical neuroanatomical
 197 homologues improved in this new latent common space. We term this the homology criterion. The locality

198 criterion tells us about our ability to extract finer-scale signal in these profiles, while the homology criterion
199 informs us about our ability to recover expected matches in this finer-scale signal. To evaluate these criteria,
200 we computed ranked similarity profiles for every region in the mouse brain, ordered such that a rank of 1
201 indicates the most similar human region. In addition, given the difference in absolute value between the
202 input gene space and gene expression latent space correlations, we scaled the similarity profiles to the interval
203 [0, 1] in order to make comparisons between the spaces.

204 We evaluated the locality criterion by examining the decay rate of the top of the similarity profiles. We
205 reasoned that the plateau of similarity to a broad brain region, as seen in the anatomically-ordered similarity
206 matrices and profiles (Figure 1, A and C; Figure 2C), would correspond to a similar plateau at the head of
207 the rank-ordered profiles. Moreover, the emergence of local signal would manifest as an increase in the range
208 between the peaks and troughs within the broad region. In the rank-ordered profiles, this would correspond
209 to a faster rate of decay at the head of the profile. In order to quantify this decay, we computed the rank
210 at which each region's similarity profile decreased to a scaled value of 0.75. This was calculated for every
211 mouse region in the initial gene space, as well as in each of the 500 gene expression latent spaces. As a
212 measurement of performance between the two representations of the data, we then took the difference in this
213 rank between each of the latent spaces and the original gene space (Figure 3A). A negative rank difference
214 indicates an improvement in the latent space.

215 Examining the structure-wise distributions of these rank differences, we found that for the majority of regions
216 in our mouse atlas, the classification approach resulted in either an improvement in the amount of locality
217 within a broad region, or no difference from the original gene space (Figure 3, B and C). Specifically, 47
218 regions (70.1%) had a mean rank difference less than or equal to zero. Additionally, the same number of
219 regions returned non-positive rank differences in at least 80% of latent spaces. A few regions performed
220 considerably worse in the latent spaces, notably the main olfactory bulb ($\mu = 18.4$; $\sigma = 12.7$), the accessory
221 olfactory bulb ($\mu = 8.7$; $\sigma = 11.6$), and the cerebellar nuclei ($\mu = 9.1$; $\sigma = 8.5$). In particular, the main
222 olfactory bulb performed worse in 96.6% of latent spaces. Regions within the cortical subplate and olfactory
223 areas (e.g. endopiriform nucleus, postpiriform transition area) benefited the most from the classification
224 approach, with many regions showing improvements in all latent spaces. While the effects are smaller, the
225 similarity profiles of regions belonging to the isocortex and cerebellar cortex also saw an improvement in
226 locality. In the isocortex, 16 out of 19 regions (84.2%) improved in at least 96% of latent spaces. In the
227 cerebellar cortex, 73.3% of regions saw a similar improvement. In contrast, regions belonging to the cerebral
228 nuclei, the diencephalon, midbrain and hindbrain did not see much improvement in this new common space.
229 For instance, only 13.2% of latent spaces returned a non-positive rank difference in the thalamus. For many

such regions the degree of locality appears to be worse in this space, though only by a small number of ranks (e.g. striatum ventral region, thalamus, midbrain raphe nuclei). Indeed, the mean rank difference and standard deviation over these regions and all latent spaces are $\mu = 1.4$ and $\sigma = 3.6$. These results demonstrate that the supervised learning approach used here can improve the resolution of neuroanatomical correspondences between the mouse and human brains, though the amount of improvement varies over the brain. Regions that were already well-characterized using the initial set of homologous genes (e.g. subcortical regions) did not benefit tremendously, but numerous regions in the cortical plate and subplate, as well as the cerebellum, saw an improvement in locality in this new common space.

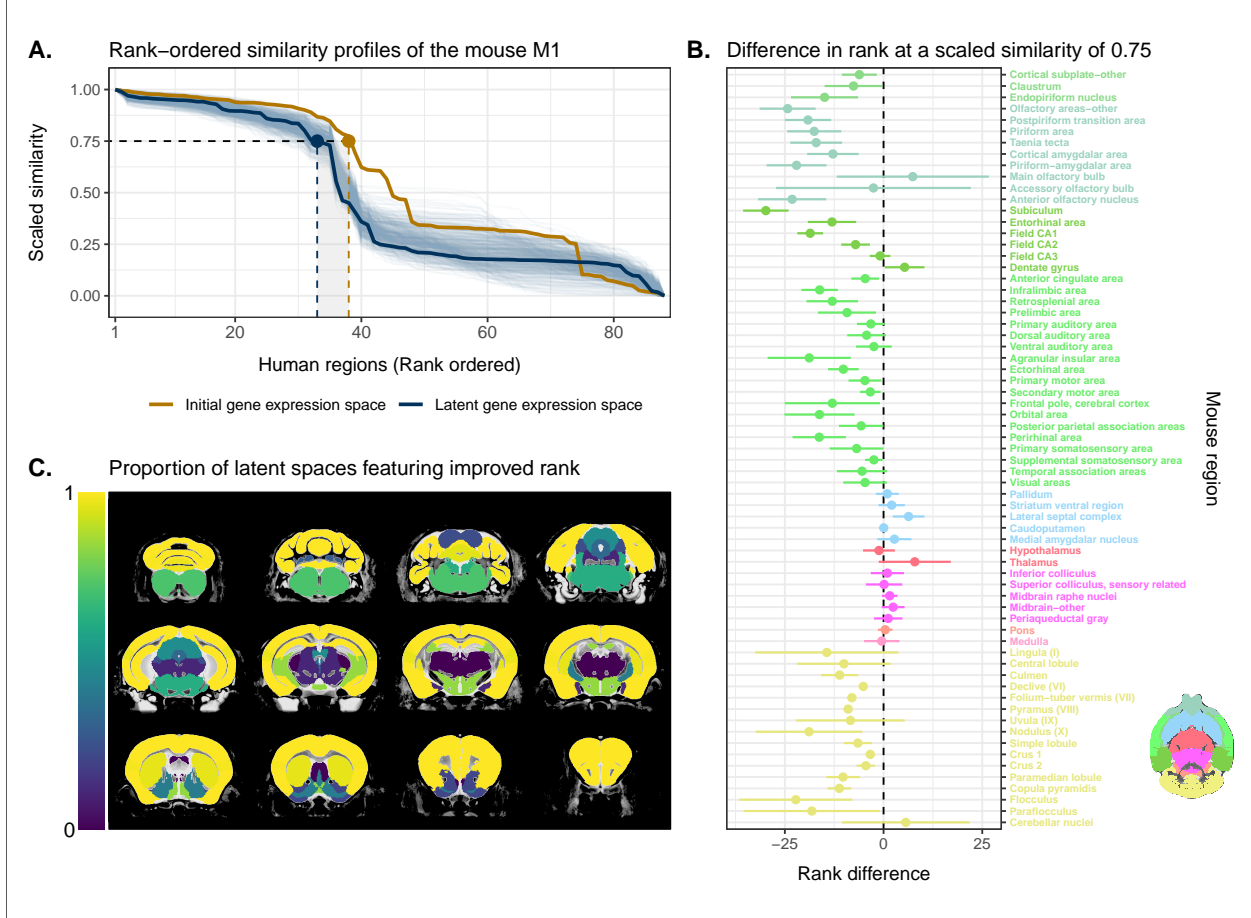


Figure 3. Quantifying improvement in locality in gene expression latent space. **(A)** The amount of local signal within a broadly similar region of the brain for a finer seed region's (e.g. primary motor area) similarity profile can be quantified by the decay rate of the head of the rank-ordered profile. Decay rate was quantified by computing the rank at a similarity of 0.75. This metric was compared between the initial gene expression space (orange line) and every gene expression latent space resulting from repeated training of the neural network (every blue line is a training outcome, heavy blue line serves as an example). A negative difference between these rank metrics indicates an improvement in locality in the latent space. **(B)** Structure-wise distributions of differences in rank at a similarity of 0.75 between the initial gene expression space and the gene expression latent spaces. Points and error bars represent mean and 95% confidence interval. Dashed black line at 0 indicates the threshold for improvement in one space over the other. Colours correspond to AMBA annotations as in Figures 1 and 2. **(C)** Proportion of perceptron training runs resulting in an improvement or null difference in the gene expression latent space compared with the initial space. Cortical and cerebellar regions exhibit high proportions of improvement, while subcortical regions are less likely to be improved by the classification process.

While the supervised learning approach improved our ability to identify matches on a finer scale for a number

239 of brain regions, this does not necessarily mean that those improved matches are biologically meaningful. The
240 second criterion for evaluating the performance of the neural network addresses whether this improvement
241 in locality captures what we would expect in terms of known mouse-human homologies. To this end, we
242 examined the degree of similarity between established mouse-human neuroanatomical pairs, both in the
243 initial gene expression space and in the set of latent spaces. We began by establishing a list of 36 canonical
244 mouse-human homologous pairs on the basis of common neuroanatomical labels in our atlases. For each of
245 these regions in the mouse brain, we compared the rank of the canonical human match in the rank-ordered
246 similarity profiles between the latent spaces and the original gene expression space (Figure 4A). The lower
247 the rank, the more similar the canonical pair, with a rank of 1 indicating maximal similarity. We additionally
248 calculated the proportion of latent spaces in which each mouse region was more similar or as similar to its
249 canonical human match compared with the initial gene space (Figure 4B).

250 We find that for most regions in this subset, the classification approach either improves the correspondence or
251 performs as well as the full set of homologous genes. For example, 73% of regions exhibit improved similarity
252 in at least 80% of latent spaces. The improvement is most pronounced for regions in the cortical subplate and
253 isocortex. In particular, the visual areas improve from a rank of 32 to an average of 10, though the variance
254 is much higher in this case. Many regions in the sub-cortex do not benefit from the gene expression latent
255 spaces since the initial gene set was already recapitulating the appropriate match with maximal similarity.
256 Apart from the pallidum and the medulla, each of these regions is maximally similar to its canonical match
257 in at least 90% of latent spaces. In such cases, the classification approach performs as well as the original
258 approach. Finally, although many regions in the cerebellum feature some improvement in the latent spaces,
259 the variation in the rank of the standard human pair is often quite large, indicating some instability in the
260 neural network's ability to recover these matches. However, while the rank of the canonical pair varies in
261 different instances of the latent space, the top matches for any given cerebellar region are always cerebellar
262 regions. For instance, when the mouse crus 1 is used as the seed region, the human crus 1 is most often
263 assigned a rank between 6 and 9. However, similar proportions in that range occur for the crus 2 and lobules
264 V, VI and VIIIB, indicating that these cerebellar regions are swapping ranks in the different latent spaces.
265 Thus while cerebellar regions are reliably associated with other cerebellar regions in the gene expression
266 latent spaces, these associations are not stable over multiple training runs.

267 Together, these results demonstrate that the multi-layer perceptron classification approach improves our abil-
268 ity to resolve finer scale mouse-human neuroanatomical matches within the broadly similar regions obtained
269 using the initial gene expression space. By training a classifier to predict the atlas labels in one species, we
270 were able to generate a new common space that amplified the amount of local signal within broadly similar

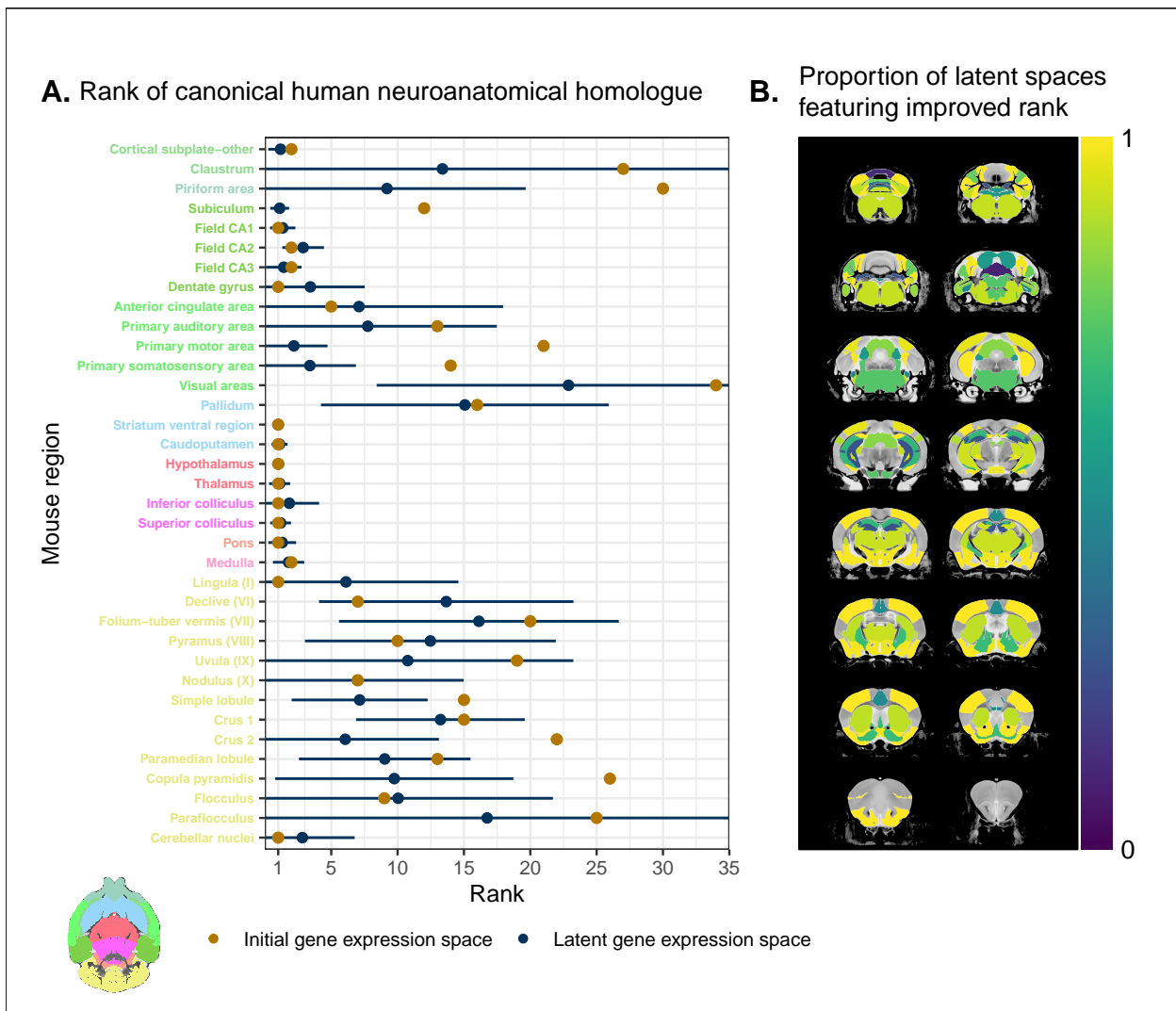


Figure 4. Recovering canonical neuroanatomical pairs in gene expression space. **(A)** Comparison between the ranks of canonical human matches for mouse seed regions between the initial gene expression space and gene expression latent spaces. Points and error bars represent mean and 95% confidence interval. Mouse region names are coloured according to the AMBA palette. **(B)** Proportion of latent spaces resulting in an improvement or null difference compared with the initial gene space. Uncoloured voxels correspond to regions with no established canonical human match.

271 regions while also improving our ability to recover known mouse-human neuroanatomical pairs.

272 **Cortical areas involved in sensorimotor processing show greater transcriptomic**
273 **similarity than supramodal areas**

274 It is well established that the brains of most, if not all, extant mammalian species follow a common organi-
275 zational blueprint inherited from an early mammalian ancestor (Kaas, 2011a). A number of cortical subdivi-
276 sions have consistently been identified in members of many distantly related mammalian species (Krubitzer,
277 2007) and hypothesized to have been present in the common ancestor of all mammals (Kaas, 2011a). While
278 it is clear that basic sensorimotor cortical regions are found in the majority of mammals, including mice and
279 humans, there is much debate about the extent to which cortical areas involved in supramodal processing
280 are conserved across mammalian taxa. Although some supramodal regions were likely present in the earliest
281 mammals, including some cingulate regions and an orbitofrontal cortex (Kaas, 2011a), since the divergence
282 of mouse and human lineages some 80 million years ago, the primate neocortex has undergone substantial
283 expansion and re-organization (Kaas, 2012). Indeed, when comparing the human neocortex even to primate
284 model species, this is the likely locus of areas that cannot be easily translated between species (Rogier B.
285 Mars et al., 2018b). As a result, it is important to investigate whether our between-species mapping is more
286 successful in somatosensory areas than supramodal areas.

287 We assessed the similarity between mouse and human isocortical areas using the pairwise correlations in each
288 of the gene expression latent spaces returned from the multi-layer perceptron. For every region in the mouse
289 isocortex, we evaluated the distribution of maximal correlation values over latent spaces (Figure 5A). While
290 the region-wise variance for each isocortical area was large, we found that, on average, sensorimotor regions
291 exhibited higher maximal correlation values than supramodal regions. The mouse primary somatosensory and
292 motor areas have the highest average maximal correlation values, with $r = 0.94 \pm 0.04$ and $r = 0.93 \pm 0.04$
293 respectively. We additionally examined the distributions of maximal correlation, grouped by cortex type
294 (Figure 5B). To generate these distributions, we computed average maximal correlation values by cortex
295 type in each of the latent spaces. Here too we find that sensorimotor regions are associated with higher
296 maximal correlation values on average ($r = 0.89 \pm 0.04$), compared with supramodal areas ($r = 0.85 \pm 0.03$).
297 These distributions demonstrate that sensorimotor isocortical regions exhibit more similarity overall on the
298 basis of homologous gene expression than do supramodal regions.

299 While we found that sensorimotor isocortical areas in the mouse brain were more similar to human brain
300 regions than supramodal areas, the distributions of maximal correlation do not speak to the neuroanatomical

301 patterns of organization for these matches. To understand how the similarity patterns of mouse and human
302 cortical subdivisions were organized, we used hierarchical clustering to cluster mouse and human isocortical
303 regions on the basis of their similarity profiles in the average gene expression latent space (Figure 5C). This
304 allows us to examine the similarity of regions to one another within and across brains at multiple levels
305 simultaneously.

306 At a high level, we find a striking segregation of the mouse isocortex into one main cluster that corresponds
307 to regions that are primarily engaged in sensorimotor processing and separate clusters of regions that are
308 supramodal. All of the sensorimotor areas cluster together, but three supramodal areas also form part of this
309 cluster: the retrosplenial area, the posterior parietal association areas, and the anterior cingulate cortex. Of
310 these, the retrosplenial area is the most different, being the first to separate out from the other regions. In
311 fact, the retrosplenial area is the mouse isocortical region with the smallest correlation values (Figure 5A).
312 The mouse sensorimotor cluster is characterized by high correlation values to human sensorimotor regions
313 like the precentral gyrus, the cuneus, and the postcentral gyrus, as well as low correlation values to the
314 piriform cortex and paraterminal gyrus.

315 At this level of clustering, the remaining mouse supramodal subdivisions form two clusters. These both
316 exhibit low similarity to the human somatosensory and visual areas, but the cluster containing the infral-
317 imbic and perirhinal areas additionally exhibits low correlation values with the precentral gyrus, anterior
318 paracentral lobule, and transverse gyri. The human cortical regions do not segregate as cleanly into senso-
319 rimotor and supramodal clusters. Under a similar level of description of four clusters of areas, the majority
320 of areas belong to a large cluster that includes a mix of cortical types. However, at a lower level of the
321 hierarchy, if the number of clusters is increased to five, this large cluster breaks up into two smaller clusters
322 that feature some delineation between supramodal and sensorimotor areas, which are primarily motor and
323 auditory in nature (e.g. precentral gyrus, Heschl's gyrus). Interestingly, the postcentral gyrus, i.e. primary
324 somatosensory area, forms a separate cluster with a set of visual areas such as the cuneus and lingual gyrus.
325 These regions exhibit very similar correlation profiles to the mouse isocortical regions, including maximal
326 correlation to the mouse primary somatosensory area, with an average of $r = 0.92$. The cluster is character-
327 ized by high correlations to the mouse sensorimotor cluster and low correlations to the mouse supramodal
328 clusters. Overall the human sensorimotor isocortical regions are loosely organized in clusters that contain
329 sensory-visual areas and auditory-motor areas.

330 We additionally ran hierarchical clustering on the isocortical similarity matrix in the original homologous
331 gene space. While the cluster annotations were not substantially different in this space, we observed that
332 the Euclidean distances within and between clusters were smaller compared with the latent space clustering,

333 further confirming that the perceptron classification approach improves the segregation of brain regions in
 334 the gene expression common space (Figure 5D).

335 Overall, we observe a greater degree of similarity between mouse and human cortical regions involved in
 336 basic sensorimotor processing compared with supramodal or association areas. This is in line with the large
 337 body of existing research that suggests that sensory and motor areas of the cortex are conserved across the
 338 brains of mammals. While sensorimotor areas exhibit a greater degree of similarity than supramodal areas,
 339 the neuroanatomical pattern of correspondences obtained using mouse-human homologous genes is not at
 340 the level of individual cortical areas. Still, using a clustering approach we identified clear distinctions in
 341 the patterns of similarity between sensorimotor and supramodal areas, especially for regions in the mouse
 342 isocortex.

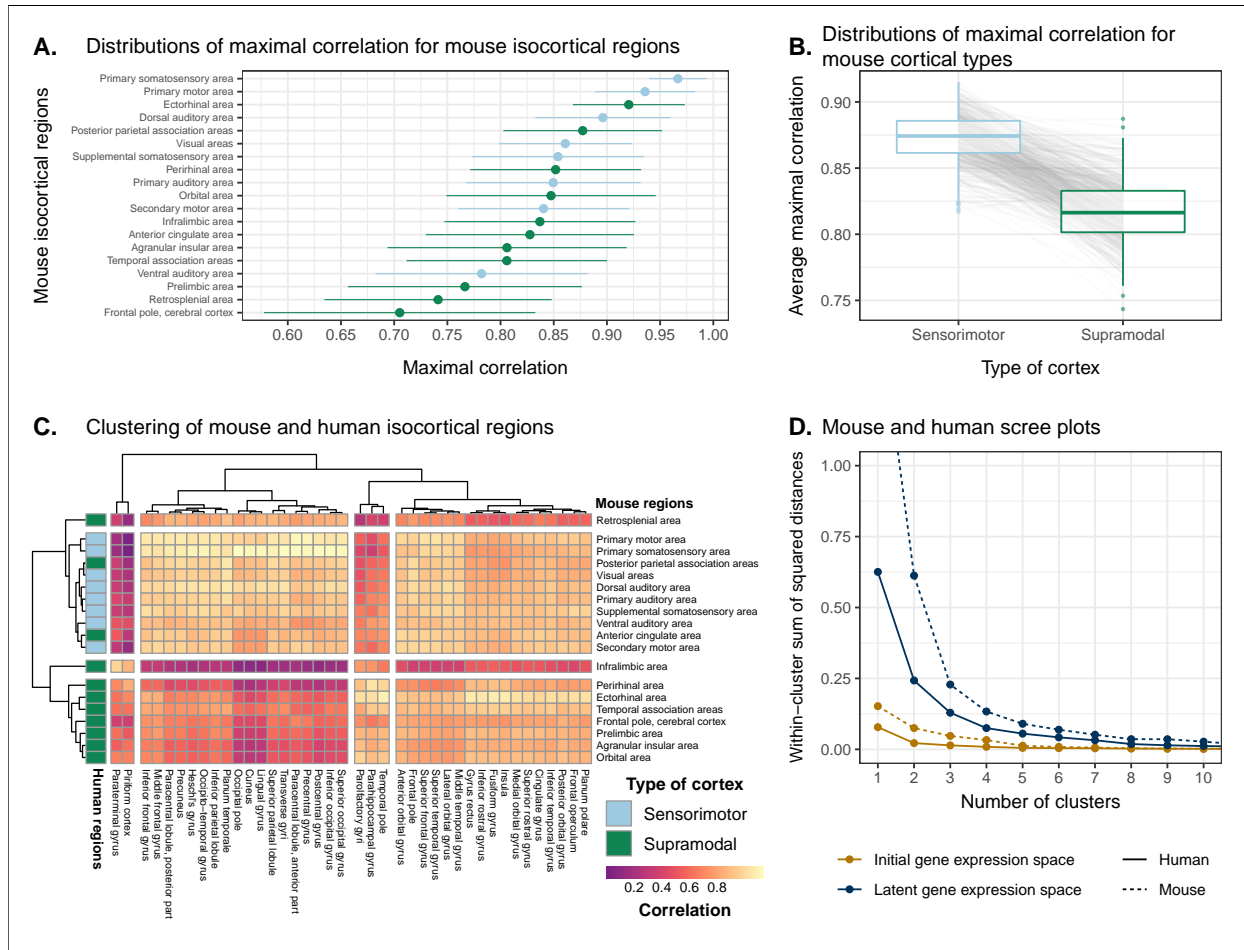


Figure 5. Similarity of mouse-human isocortical regions. **(A)** Maximal correlation distributions of mouse isocortical regions. Points and error bars represent mean and 95% confidence interval over latent space samples. **(B)** Distributions of average maximal correlation for sensorimotor and supramodal isocortical areas in each gene expression latent space. Grey lines correspond to individual latent spaces. **(C)** Hierarchical clustering of mouse and human isocortical regions based on average latent space correlation values. Mouse regions are annotated as sensorimotor or supramodal. Four clusters were chosen for visualization using the elbow method. **(D)** Within-cluster sum of squared distances for different numbers of mouse and human isocortical clusters in the average latent space and initial homologous gene space.

³⁴³ **Transcriptomic comparison of the mouse and human striatum**

³⁴⁴ We have focused here on comparing mouse and human brain organization using transcriptomic data, with
³⁴⁵ a latent space based on homologous genes as the common space between the two species. To date, common
³⁴⁶ space comparisons between the mouse and human brain have only been performed using functional con-
³⁴⁷nectivity (Balsters et al., 2020; Schaeffer et al., 2020). As a case in point, Balsters et al. (2020) compared
³⁴⁸ mouse and human striatal organization using this measure. They found that the nucleus accumbens was
³⁴⁹ highly conserved between mice and humans, and that voxels in the posterior part of the human putamen
³⁵⁰ were significantly similar to the lateral portion of their mouse caudoputamen parcellation. Additionally,
³⁵¹ they report that 85% of voxels in the human striatum were not significantly similar to any of their mouse
³⁵² striatal seeds, and that 25% of human striatal voxels were significantly dissimilar compared with the mouse.
³⁵³ These differences were understandable, as they involved parts of the human striatum that connected to parts
³⁵⁴ of prefrontal cortex that have no known homolog in the mouse (Neubert et al., 2014). However, it is not
³⁵⁵ necessarily the case that between-species differences in connectivity are associated with distinct architectonic
³⁵⁶ or molecular signatures. Therefore, we investigated the patterns of similarity between the mouse and human
³⁵⁷ striata on the basis of gene expression using the neural network latent space representations.

³⁵⁸ We first identified the striatal regions present in the Allen human dataset: the caudate, the putamen, and the
³⁵⁹ nucleus accumbens. We evaluated the correlation between the microarray samples in these regions and every
³⁶⁰ region in the mouse atlas. Based on these correlation values, we focused our analysis on the four mouse
³⁶¹ regions that were consistently the most similar across all latent spaces: the caudoputamen, the nucleus
³⁶² accumbens, the fundus of striatum, and the olfactory tubercle. For each of the human striatal regions, we
³⁶³ then calculated the average correlation over the samples to each of the mouse targets. We examined the
³⁶⁴ distribution of these average correlation values over the latent spaces (Figure 6A). We find that the human
³⁶⁵ caudate and putamen consistently exhibit the strongest degree of similarity to the mouse caudoputamen.
³⁶⁶ The median of the distribution for the caudate-caudoputamen pairs is 0.95 and 0.97 for the putamen-
³⁶⁷ caudoputamen pairs, with modal values of 0.94 and 0.97, respectively. All latent spaces return correlations
³⁶⁸ greater than 0.9 for caudate-caudoputamen and putamen-caudoputamen pairs. Beyond this expected top
³⁶⁹ match, the caudate and putamen both exhibit high similarity to the nucleus accumbens and the fundus of
³⁷⁰ striatum, with mean correlation values of about 0.80. Neither of these target regions is consistently more
³⁷¹ similar to the mouse caudoputamen over all latent spaces.

³⁷² While the similarity of the caudate and the putamen to the caudoputamen is unsurprising, the story is not
³⁷³ as clear for the human nucleus accumbens. We find that the variance in correlation calculated over all mouse

374 targets is much lower ($\sigma = 0.04$) compared with the equivalent variances for the caudate ($\sigma = 0.09$) and
375 putamen ($\sigma = 0.10$), indicating less specificity to any one mouse striatal target. In particular, the human
376 nucleus accumbens isn't as specifically similar to the mouse nucleus accumbens in the way that the caudate
377 and putamen are similar to the caudoputamen. The mouse target distributions are right-shifted compared
378 with those for the caudate and putamen, with mean values of 0.90, 0.89, and 0.89 for the mouse nucleus
379 accumbens, caudoputamen, and fundus of striatum, respectively. The human accumbens also exhibits a high
380 degree of similarity to the mouse olfactory tubercle, the distribution of which is also right-shifted compared
381 with the caudate and putamen.

382 Given the high correlation of the human caudate and putamen to the mouse caudoputamen, as well as the
383 finding reported by Balsters et al. about the similarity of the lateral caudoputamen to the putamen, we were
384 curious as to whether we could identify sub-regional patterns of similarity in the caudoputamen and other
385 striatal regions using these gene expression data. To probe this question, we first examined the average latent
386 space correlation between each voxel in the mouse striatum and every region in the human atlas. We created
387 brain maps for the human regions that exhibited the highest mean correlation values, averaged over mouse
388 striatal voxels: the caudate, the putamen, the nucleus accumbens, and the septal nuclei (Figure 6B). We find
389 that voxels in the caudoputamen exhibit a homogeneous pattern of similarity to both the caudate and the
390 putamen. On average, voxels in the caudoputamen have a correlation of 0.95 to the caudate and 0.94 to the
391 putamen, with standard deviations of 0.04 and 0.05 respectively. The caudate and putamen are associated
392 with correlations of at least 0.90 in 88% and 84% of caudoputamen voxels. A number of voxels are also
393 highly similar to the human nucleus accumbens, with an average correlation value of 0.90 and 55% of voxels
394 returning a correlation of at least 0.9. The caudoputamen voxels most similar to the nucleus accumbens lie
395 in the ventral-rostral part of the region. Of course, voxels in the mouse nucleus accumbens are also highly
396 similar to the human nucleus accumbens, with an average of 0.90 and standard deviation of 0.06. While the
397 human nucleus accumbens is the most strongly correlated region, a number of voxels also exhibit reasonably
398 strong correlations to the substantia innominata, the septal nuclei, and the amygdala. Indeed, 91% of voxels
399 in the accumbens are correlated at a value of 0.7 or higher to the substantia innominata. The equivalent
400 percentages for the septal nuclei and amygdala are 78% and 74% respectively.

401 We additionally examined the proportion of latent spaces in which each voxel in the mouse striatum was
402 maximally similar to the human target regions (Figure 6C). As expected, we find that voxels in the cau-
403 doputamen are most often maximally similar to the human caudate and putamen, with 75% of voxels in
404 the caudoputamen being maximally similar to the caudate or putamen in at least 95% of latent spaces, and
405 62% of voxels being maximally similar to one of those targets in all latent spaces. Interestingly, we observe

406 the emergence of a continuous bilateral pattern of specificity to the caudate and putamen, with voxels in
407 the rostral and lateral-caudal parts of the caudoputamen being more specific to the caudate, and voxels in
408 the medial-rostral part being more specific to the putamen. This map highlights subtle differences in the
409 similarity between caudoputamen voxels and the caudate or putamen. While this pattern distinguishes the
410 two regions on the basis of which is the top match, individual voxels have very similar correlation values to
411 the targets (Figure 6B), with a mean difference in correlation of only 0.006. Beyond the caudoputamen, we
412 find that the accumbens and olfactory tubercle in the mouse are consistently similar to the human nucleus
413 accumbens, with 80% of mouse accumbens voxels and 65% of olfactory tubercle voxels having the human
414 accumbens as their top match in at least 80% of latent spaces. For those voxels below this threshold, the
415 human regions that are most often the top match are once again the amygdala, the septal nuclei, and the
416 substantia innominata.

417 Overall, we observe a strong association between the mouse caudoputamen and both the human caudate and
418 putamen. While we find a subtle pattern of specificity to either region among voxels in the caudoputamen on
419 the basis of maximal similarity, the high degree of similarity in the correlation values to each region suggests
420 that the majority of voxels in the caudoputamen are equally similar to the caudate and the putamen on the
421 basis of the expression of mouse-human homologous genes. We also find that the nucleus accumbens is well
422 conserved across species. However the region also exhibits patterns of similarity that go beyond the simple
423 one-to-one match. The human accumbens features similar correlation values to the mouse caudoputamen
424 and fundus of striatum, in addition to the accumbens proper, with no sharp distinction between these regions.
425 It also exhibits a larger degree of similarity to the mouse olfactory tubercle. This is also seen in the mouse
426 striatum, where voxels in the accumbens and the olfactory tubercle map onto the human accumbens.

427 Discussion

428 We have demonstrated how spatial transcriptomic patterns of homologous genes can be used to make quan-
429 titative comparisons between the mouse and human brain. We showed that using homologous genes as a
430 common space allows one to easily identify coarse similarities in brain structures across species, but that
431 more fine-scaled parcellations, such as at the level of cortical areas, are more complex. Despite this limi-
432 tation, the approach still allows for a formal assessment of different patterns of between-species similarity
433 in primary compared to supramodal regions, identifications of distinct clusters of cortical territories across
434 species, and comparison of between-species similarities at the transcriptomic level to those observed using
435 other modalities. We will discuss our observations in the context of the importance of the mouse as a model

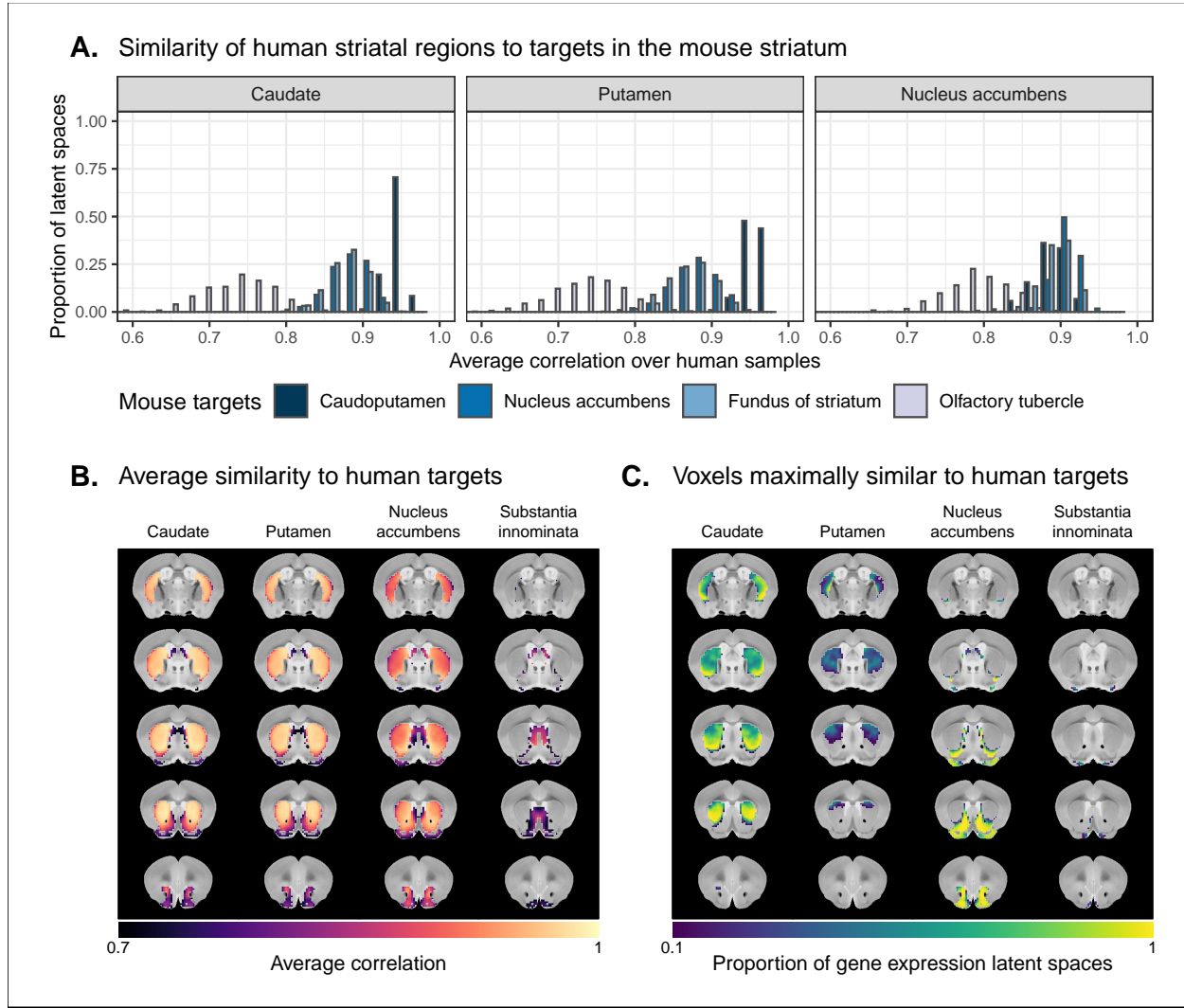


Figure 6. Similarity among mouse and human striatal regions. **(A)** Distributions over gene expression latent spaces of region-wise average correlation values for mouse and human striatal pairs. Human regions were chosen based on the AHBA ontology. Mouse target regions were chosen to be those with the highest average correlation values. **(B)** Latent space averaged correlations between voxels in the mouse striatum and human target regions. Target regions were selected based on the highest mean correlation across all striatal voxels. **(C)** Proportions of latent spaces in which mouse striatal voxels are maximally similar to human target regions.

436 for human neuroscience below.

437 The abundance of neuroscience research performed using mice has resulted in a wealth of knowledge about the
438 mouse brain. In the preclinical setting, mouse models are utilized with the intention of better understanding
439 human neuropathology. For instance, in the context of autism spectrum disorders, a plethora of studies
440 using mouse models have reported on the neurobiological and neuroanatomical phenotypes that arise from
441 mutations at specific genetic loci (Gompers et al., 2017; Horev et al., 2011; Pagani et al., 2021). It is common
442 for researchers involved in translational neuroscience to rely on findings of this kind to make inferences about
443 the human disorder. The typical approach, which is to identify rough post-hoc correspondences between
444 neuroanatomical ontologies, is not particularly comprehensive and is subject to confirmation bias. While it
445 may be a reasonable starting point for comparison, the true correspondence between the mouse and human
446 brain is likely more complicated given the evolutionary distance between the two species. Although overall
447 patterns of brain organization, including the general pattern of neocortical organization, are similar across
448 all mammals, substantial differences are evident (Ventura-Antunes et al., 2013). To make matters worse,
449 researchers from the different neuroscientific traditions often use distinct terminology, further complicating
450 detailed information exchange. To address these problems, we sought to establish a first quantitative whole-
451 brain comparison between the two species.

452 The expression of homologous genes provides an elegant way to define a common space for quantitative cross-
453 species comparisons since it relies on homology at a deep molecular biological level. The approach is not
454 without limitations however. First, the acquisition of whole-brain transcriptomic data is labour-intensive,
455 time consuming, and invasive. These data sets cannot be generated easily, especially in the human, in which
456 the process depends on the availability of post-mortem samples. As a result, the effective sample sizes are
457 extremely limited in this domain. For instance, in the Allen mouse coronal in-situ hybridization data set
458 used here, the brain-wide expression of each gene is sampled only once (barring a few exceptions). This
459 constrains the types of analyses that are possible (e.g. null hypothesis significance testing) and largely limits
460 the availability of replication data sets. That being said, new technologies, such as spatial transcriptomics,
461 are gradually making it easier to acquire brain-wide gene expression data in less time and at lower cost (Ortiz
462 et al., 2020; Stahl et al., 2016; Vickovic et al., 2019). Second, the approach of relying on all available genes
463 is subject to noise. To address this issue, Myers (2017) (Myers, 2017) used a method of gene set selection
464 to attempt to improve the correspondence between established mouse-human homologies. While this lead
465 to improvement, it was only at the level of coarsely defined regions (e.g. cortex-cortex). Our approach,
466 therefore, was to use supervised machine learning to create a latent common space based on combinations
467 of homologous genes that can delineate areas within a single species.

468 This latent common space approach led to a substantial improvement in specificity of between-species com-
469 parisons. Nevertheless, it is evident that the first major distinction in gene expression patterns within a
470 species, and the easiest identification of similarity across species, is at the coarse anatomical level of the
471 major subdivisions of the vertebrate brain, such as the isocortex, cerebellar hemispheres and nuclei, and
472 brain stem. All of these territories were present in the ancestral vertebrate brain (Striedter and Northcutt,
473 2020) and the ability to detect conserved transcriptomic signatures at this level is not surprising. Within
474 such structures, such as the isocortex, our ability to make simple one-to-one correspondences decreased. This
475 is partly because areas within a coarse structure have more similar transcriptomic profiles, but also likely
476 due to the fact that a single area in one brain does not have a single correspondent in another, larger brain.
477 In other words, regions in the brains of related species may exhibit one-to-many or many-to-many mappings.
478 In our study, we found greater cross-species similarity between cortical areas associated with sensorimotor
479 processing than areas in supramodal cortex. Primary areas, including the sensorimotor areas, are present
480 in all mammals studied to date and likely part of the common ancestors of all mammals (Kaas, 2011a;
481 Krubitzer, 2007). Although this common ancestor likely also had non-primary areas, it cannot be denied
482 that association cortex expanded dramatically in primates and especially so in the human brain (Chaplin et
483 al., 2013; Mars et al., 2016a). Again, the pattern found here of greater similarity in more conserved areas
484 might reflect this evolutionary history. In that context it is interesting to note that some non-primary areas
485 thought to be present in the common mammalian ancestor, such as cingulate and orbitofrontal cortex (Kaas,
486 2011a) showed relatively high correlation to human areas.

487 An advantage of the approach presented here is that it can, in principle, be applied to any aspect of brain
488 organization. Beyond simply establishing whether areas are similar across species in a particular common
489 space, comparing the results across common spaces established using different types of neuronal data can
490 inform on which larger principles of organization are similar across brains (Eichert et al., 2020). This is
491 illustrated here by the results of our striatal analysis. We found high similarity between the human caudate
492 and putamen and mouse caudoputamen, with little differentiation within these regions in a single species.
493 In contrast, Balsters et al. (2020) demonstrated that human caudoputamen contains a distinct pattern of
494 connectivity. At first sight, one could argue the results are in contrast. However, evolutionarily speaking, it
495 is quite probable that an overall similar transcriptomic signature of the striatum can be accompanied by a
496 distinct connectivity pattern to areas of the cortex present in only one of the two species. Indeed, this speaks
497 to the different types of similarity that can be studied, depending on which aspect of brain organization one
498 is interested in. Although the human brain is much larger than the mouse brain and contains a number
499 of cortical territories that have no homologue in the mouse brain (Kaas, 2011b; Rudebeck and Izquierdo,

500 2022), the similarity in transcriptomic signature mean that translations between the species is valid in many
501 contexts.

502 The power of a formal understanding of similarities and differences between brains at different levels of
503 organization is evident. In fundamental neuroscience, it will help translate results from data types that
504 cannot be obtained in humans to the human brain (Barron et al., 2021). In translational neuroscience, it
505 will, in a negative sense, help establish the limits of the translational paradigm by showing which aspects
506 of the human brain cannot be understood using the model species (Liu et al., 2021). In a positive sense,
507 it will also help by establishing and improving our understanding of the many aspects in which the model
508 and human brain do concur (Mandino et al., 2021). More ambitious still, it can provide a way in which
509 highly diverse manifestations of certain disease syndromes (e.g. autism spectrum disorder) (Grzadzinski et
510 al., 2013; Simonoff et al., 2008) and the availability of many distinct model strains (Ellegood et al., 2015),
511 each hypothesized to capture a distinct aspect of a multi-dimensional clinical syndrome, can be related to
512 one another. Ultimately, we believe that using the mapping of homologous gene expression between species
513 can be an important part of building a transform that maps information obtained using mice to humans and
514 vice versa.

515 Materials and methods

516 Mouse gene expression data

517 We used the adult mouse whole-brain in-situ hybridization data sets from the Allen Mouse Brain Atlas
518 (Lein et al., 2007). Specifically, we used 3D expression grid data, i.e. expression data aligned to the Allen
519 Mouse Brain Common Coordinate Framework (CCFv3)(Wang et al., 2020) and summarized under a grid
520 at a resolution of $200\mu\text{m}$. We downloaded the gene expression “energy” volumes from both the coronal
521 and sagittal in-situ hybridization experiments as a sequence of 32-bit float values using the Allen Institute’s
522 API (<http://help.brain-map.org/display/api/Downloading+3-D+Expression+Grid+Data>). These volumes
523 were subsequently reshaped into 3D images in the MINC format. Origin, extents, and spacing were defined
524 such that the image was RAS-oriented, with the origin at the point where the anterior commissure crosses
525 the midline. The MINC images from the coronal and sagittal data sets were then processed separately
526 using the Python programming language. The sagittal data set was first filtered to keep only those genes
527 that were also present in the coronal set. Images were imported using the `pyminc` package, masked and
528 reshaped to form an experiment-by-voxel expression matrix. We pre-processed this data by first applying a

529 `log2` transformation for consistency with the human data set. For those genes associated with more than
530 one in-situ hybridization experiment, we averaged the expression of each voxel across the experiments. We
531 subsequently filtered out genes for which more than 20% of voxels contained missing values. Finally, we
532 applied a K-nearest neighbours algorithm to impute the remaining missing values. The result of this pre-
533 processing pipeline was a gene-by-voxel expression matrix with 3958 genes and 61315 voxels for the coronal
534 data set and a matrix with 3619 genes and 26317 voxels for the sagittal data set.

535 Human gene expression data

536 Human gene expression data was obtained from the Allen Human Brain Atlas (Hawrylycz et al., 2012).
537 The data were downloaded from the Allen Institute’s API (<http://api.brain-map.org>) and pre-processed
538 using the `abagen` package in Python (<https://abagen.readthedocs.io/en/stable/>) (Arnatkeviciūtė et al., 2019;
539 Hawrylycz et al., 2012; Markello et al., 2021). We used the microarray data from the brains of all six donors,
540 each of which contains `log2` expression values for 58692 gene probes across numerous tissue samples. The
541 pre-processing pipeline included probe selection using differential stability on data from all donors and
542 intensity-based filtering of probes at a threshold of 0.5. The samples and genes were additionally normalized
543 for each donor individually using a scaled robust sigmoid function. In practice, this pipeline was implemented
544 using the `get_samples_in_mask` function from the `abagen` package. The remaining parameters were set to
545 their default values. The output of the pre-processing pipeline was a gene-by-sample expression matrix with
546 15627 genes and 3702 samples across all donors.

547 Mouse atlases

548 We used a version of the DSURQE atlas from the Mouse Imaging Centre (Dorr et al., 2008; Qiu et al., 2018;
549 Richards et al., 2011; Steadman et al., 2014; Ullmann et al., 2013), modified using the AMBA hierarchical
550 ontology, which was downloaded from the Allen Institute’s API. The labels of the DSURQE atlas correspond
551 to the leaf node regions in the AMBA ontology, which allowed us to use the hierarchical neuroanatomical
552 tree to aggregate and prune the atlas labels to the desired level of granularity. For the purposes of our
553 analyses, we removed white matter and ventricular regions entirely. The remaining grey matter regions were
554 aggregated up the hierarchy so that the majority of resulting labels contained enough voxels to be classified
555 appropriately by the multi-layer perceptron. In doing so, we maintained approximately the same level of
556 tree depth within a broad region (e.g. cerebellar regions were chosen at the same level of granularity). This
557 resulted in a mouse atlas with 67 grey matter regions. We additionally generated an atlas with 11 broader

558 regions for visualization and annotation purposes.

559 Human atlases

560 We used the hierarchical ontology from the AHBA, which we obtained using the Allen Institute’s API.
561 We aggregated and pruned the neuroanatomical hierarchy to correspond roughly to the level of granularity
562 obtained in our mouse atlas, resulting in 88 human brain regions. We additionally generated a set of 16
563 broad regions for visualization and annotation. White matter and ventricular regions were omitted entirely.

564 Regional expression and similarity matrices

565 We created the mouse and human gene-by-region expression matrices from the mouse gene-by-voxel and
566 human gene-by-sample expression matrices. First, we intersected the gene sets in these matrices with a
567 list of 3331 homologous genes obtained from the NCBI HomoloGene database (NCBI, 2018), resulting in
568 2835 homologous genes present in both the mouse and human expression matrices. We then annotated
569 each of the human samples with one of the 88 human atlas regions, and each of the mouse voxels with
570 one of the 67 mouse atlas regions, discarding white matter and ventricular entries in the process. These
571 labelled expression matrices were subsequently normalized as follows: For each matrix, we first standardized
572 every gene across all voxels/samples using a z-scoring procedure. We then centered every voxel/sample
573 by subtracting the average expression over all homologous genes. Finally, we generated the gene-by-region
574 expression matrices by averaging the expression of every gene over the voxels/samples corresponding to
575 each atlas region. Using these expression matrices, we generated the mouse-human similarity matrix by
576 computing the Pearson correlation coefficient between all pairs of mouse and human regions.

577 Gene enrichment analysis

578 We ran a gene enrichment analysis on the set of homologous genes obtained from the NCBI HomoloGene
579 database. We first downloaded Gene Ontology data for biological process related modules from the Bader
580 Lab at the University of Toronto (<http://baderlab.org/GeneSets>). These data include a gene set of 16563
581 genes and a module set of 15757 biological process modules. Every module is associated with a subset
582 of genes from the full gene set. For each module, we used a hypergeometric test to evaluate whether the
583 homologous gene set was over-represented in the module subset, compared with the full gene set. The
584 resulting p-values were adjusted for multiple comparisons using the false-discovery rate method (Benjamini

585 and Hochberg, 1995). A total of 938 modules were found to be significant at a threshold of 0.001. The
586 surviving modules were ordered according to their p-values and written out to a comma-separated values
587 data file (Supplementary File 1). This analysis was carried out using the `tmod` package in the R programming
588 language.

589 Multi-layer perceptron classification and latent space

590 To improve the resolution of mouse-human neuroanatomical matches, we performed a supervised learning
591 approach, wherein we trained a multi-layer perceptron neural network to classify 67 mouse atlas regions
592 from the expression values of 2835 homologous genes. We chose a model architecture in which each layer
593 of the network was fully connected to previous and subsequent layers. To optimize the hyperparameters,
594 we implemented an ad hoc cross-validation procedure that took into account the fact that the majority of
595 genes in the coronal AMBA data set are sampled only once over the entire mouse brain. The procedure
596 involved a combination of the coronal data set and the sagittal in-situ hybridization data sets. For the
597 sagittal data set, we used the expression matrix described above. However, we used a modified version
598 of the coronal expression matrix. This matrix was generated using the pipeline described above with the
599 following modifications: 1. We applied a *unilateral* brain mask to the coronal images since the sagittal data
600 is unilateral by construction, and 2. we did not aggregate the expression of multiple in-situ hybridization
601 experiments for those genes in the coronal set pertaining to more than one experiment. We then filtered
602 these experiment-by-voxel expression matrices according to the list of mouse-human homologous genes, as
603 well as the human sample expression matrix. We also annotated the voxels in each of the expression matrices
604 with one of the 67 regions in the mouse atlas. Our validation procedure then involved iterative construction
605 of training and validation sets by sampling gene experiments from either the coronal or sagittal matrices: For
606 every gene in the homologous set, we first determined whether that gene was associated with more than one
607 experiment in the coronal matrix. If this was the case, we randomly sampled one of those experiments for the
608 training set and one of the remaining experiments for the validation set. If the gene was associated with only
609 one experiment in the coronal set, we randomly sampled either the coronal or sagittal experiment for the
610 training set and the other for the validation set. Once the training and validation sets were generated, they
611 were normalized using the procedure described above. We then trained the neural network using the training
612 set and evaluated its performance on the validation set. Given that the construction of the training and
613 validation sets involved some stochasticity, we repeated this construction, training, and validation procedure
614 10 times for every combination of hyperparameters.

615 The hyperparameters that we optimized using this method were the number of hidden layers in the network,

the number of hidden units (i.e. neurons) per hidden layer, the dropout rate, and the amount weight decay. The values we optimized over were as follows. We varied the number of hidden layers between 3 and 5. We varied the number of hidden units between 100 and 1000 in increments of 100. For the dropout rate, we examined values of 0, 0.25 and 0.50. For the amount of weight decay, we examined values of 10^{-6} and 10^{-5} . We found that the best-performing model had 3 hidden layers, 200 neurons per layer, a dropout rate of 0, and a weight decay value of 10^{-6} . This model returned an average classification accuracy of 0.926 on the training sets and of 0.526 on the validation sets. Following validation, we used the optimal hyperparameters to train the network on the full bilateral coronal voxel-wise expression matrix.

These models were implemented in Python using PyTorch via the `skorch` library (<https://skorch.readthedocs.io/en/stable/>). For both validation and training, the models were trained over 200 epochs using a maximum learning rate of 10^{-5} . We used the `AdamW` optimization algorithm (Loshchilov and Hutter, 2019) and `OneCycleLR` learning rate scheduler policy. The activation function used in the forward pass was the rectified linear unit (ReLU) and the loss function was the negative log-likelihood loss, which is the default for the `NeuralNetClassifier` class in `skorch`.

We used the trained perceptron to generate the latent gene expression space. To extract the appropriate transformation, we removed the predictive output layer and soft-max transformation from the network architecture. The resulting architecture returns the 200 hidden units in the third hidden layer as the output of the network. To create the latent space data representations, we applied this network to the mouse and human gene-by-region expression matrices, transposed so that the genes were the input variables. The resulting matrices have 200 columns corresponding to the hidden units and 67 (88) rows corresponding to the mouse (human) regions. They describe each brain region's weight over the hidden units. To create the similarity matrix, we calculated the Pearson correlation coefficient between all pairs of mouse and human regions.

Given the stochasticity inherent in training the network (e.g. random weight initialization and stochastic optimization), we repeated the training and transformation process 500 times using the same network architecture and input data.

642 Data and code availability

This manuscript, including all figures, was generated programmatically using R Markdown (<https://rmarkdown.rstudio.com>) and L^AT_EX(<https://www.latex-project.org>). The Allen Mouse Brain Atlas and Allen Human Brain Atlas data sets are openly accessible and can be downloaded from the

646 Allen Institute's API (<http://api.brain-map.org>). All of the code and additional data needed to gen-
647 erate this analysis, including figures and manuscript, is accessible at <https://github.com/abeaucha/>
648 MouseHumanTranscriptomicSimilarity/.

649 Acknowledgments

650 We thank C. Hammill, D.J. Fernandes, E. Anagnostou, B.J. Nieman, and E. Sibille for providing advice
651 and for interesting conceptual discussions. This study was supported by the Canadian Institutes of Health
652 Research (doctoral funding and foreign study award for A.B.). The Wellcome Centre for Integrative Neu-
653 roimaging is supported by core funding from the Wellcome Trust (203139/Z/16/Z).

654 Competing interests

655 The authors declare that they have no competing interests.

656 References

- 657 Arnatkevičiūtė A, Fulcher BD, Fornito A. 2019. A practical guide to linking brain-wide gene expression and
658 neuroimaging data. *NeuroImage* **189**:353–367. doi:10.1016/j.neuroimage.2019.01.011
- 659 Balsters JH, Zerbi V, Sallet J, Wenderoth N, Mars RB. 2020. Primate homologs of mouse cortico-striatal
660 circuits. *eLife* **9**:24. doi:10.7554/eLife.53680
- 661 Barron HC, Mars RB, Dupret D, Lerch JP, Sampaio-Baptista C. 2021. Cross-species neuroscience:
662 Closing the explanatory gap. *Philosophical Transactions of the Royal Society B: Biological Sciences*
663 **376**:20190633. doi:10.1098/rstb.2019.0633
- 664 Benjamini Y, Hochberg Y. 1995. Controlling the False Discovery Rate: A Practical and Powerful Approach
665 to Multiple Testing. *Journal of the Royal Statistical Society Series B (Methodological)* **57**:289–300.
- 666 Burt JB, Demirtaş M, Eckner WJ, Navejar NM, Ji JL, Martin WJ, Bernacchia A, Anticevic A, Murray JD.
667 2018. Hierarchy of transcriptomic specialization across human cortex captured by structural neuroimag-
668 ing topography. *Nature Neuroscience* **21**:1251–1259. doi:10.1038/s41593-018-0195-0
- 669 Chaplin TA, Yu H-H, Soares JGM, Gattass R, Rosa MGP. 2013. A Conserved Pattern of Differen-
670 tial Expansion of Cortical Areas in Simian Primates. *Journal of Neuroscience* **33**:15120–15125.
671 doi:10.1523/JNEUROSCI.2909-13.2013

- 672 Dietrich MR, Ankeny RA, Chen PM. 2014. Publication Trends in Model Organism Research. *Genetics*
673 **198**:787–794. doi:10.1534/genetics.114.169714
- 674 Dorr AE, Lerch JP, Spring S, Kabani N, Henkelman RM. 2008. High resolution three-dimensional brain
675 atlas using an average magnetic resonance image of 40 adult C57Bl/6J mice. *NeuroImage* **42**:60–69.
676 doi:10.1016/j.neuroimage.2008.03.037
- 677 Eichert N, Robinson EC, Bryant KL, Jbabdi S, Jenkinson M, Li L, Krug K, Watkins KE, Mars RB. 2020.
678 Cross-species cortical alignment identifies different types of anatomical reorganization in the primate
679 temporal lobe. *eLife* **9**:e53232. doi:10.7554/eLife.53232
- 680 Ellegood J, Anagnostou E, Babineau BA, Crawley JN, Lin L, Genestine M, DiCicco-Bloom E, Lai JK, Y,
681 Foster JA, Peñagarikano O, Geschwind DH, Pacey LK, Hampson DR, Laliberté CL, Mills AA, Tam
682 E, Osborne LR, Kouwer M, Espinosa-Becerra F, Xuan Z, Powell CM, Raznahan A, Robins DM, Nakai
683 N, Nakatani J, Takumi T, Eede MC van, Kerr TM, Muller C, Blakely RD, Veenstra-VanderWeele J,
684 Henkelman RM, Lerch JP. 2015. Clustering autism: Using neuroanatomical differences in 26 mouse
685 models to gain insight into the heterogeneity. *Molecular Psychiatry* **20**:118–125. doi:10.1038/mp.2014.98
- 686 Ellenbroek B, Youn J. 2016. Rodent models in neuroscience research: Is it a rat race? *Disease Models &*
687 *Mechanisms* **9**:1079–1087. doi:10.1242/dmm.026120
- 688 Englund M, James SS, Bottom R, Huffman KJ, Wilson SP, Krubitzer LA. 2021. Comparing cortex-wide
689 gene expression patterns between species in a common reference frame. doi:10.1101/2021.07.28.454203
- 690 Fulcher BD, Murray JD, Zerbi V, Wang X-J. 2019. Multimodal gradients across mouse cortex. *Proceedings*
691 *of the National Academy of Sciences* **116**:4689–4695. doi:10.1073/pnas.1814144116
- 692 Gompers AL, Su-Feher L, Ellegood J, Copping NA, Riyadh MA, Stradleigh TW, Pride MC, Schaffler MD,
693 Wade AA, Catta-Preta R, Zdilar I, Louis S, Kaushik G, Mannion BJ, Plajzer-Frick I, Afzal V, Visel
694 A, Pennacchio LA, Dickel DE, Lerch JP, Crawley JN, Zarbalis KS, Silverman JL, Nord AS. 2017.
695 Germline Chd8 haploinsufficiency alters brain development in mouse. *Nature Neuroscience* **20**:1062–
696 1073. doi:10.1038/nn.4592
- 697 Grzadzinski R, Huerta M, Lord C. 2013. DSM-5 and autism spectrum disorders (ASDs): An opportunity
698 for identifying ASD subtypes. *Molecular Autism* **4**:12. doi:10.1186/2040-2392-4-12
- 699 Hawrylycz MJ, Lein ES, Guillozet-Bongaarts AL, Shen EH, Ng L, Miller JA, Lagemaat LN van de, Smith
700 KA, Ebbert A, Riley ZL, Abajian C, Beckmann CF, Bernard A, Bertagnolli D, Boe AF, Cartagena PM,
701 Chakravarty MM, Chapin M, Chong J, Dalley RA, Daly BD, Dang C, Datta S, Dee N, Dolbeare TA, Faber
702 V, Feng D, Fowler DR, Goldy J, Gregor BW, Haradon Z, Haynor DR, Hohmann JG, Horvath S, Howard
703 RE, Jeromin A, Jochim JM, Kinnunen M, Lau C, Lazarz ET, Lee C, Lemon TA, Li L, Li Y, Morris JA,
704 Overly CC, Parker PD, Parry SE, Reding M, Royall JJ, Schulkin J, Sequeira PA, Slaughterbeck CR, Smith

- 705 SC, Sodt AJ, Sunkin SM, Swanson BE, Vawter MP, Williams D, Wohnoutka P, Zielke HR, Geschwind
706 DH, Hof PR, Smith SM, Koch C, Grant SGN, Jones AR. 2012. An anatomically comprehensive atlas of
707 the adult human brain transcriptome. *Nature* **489**:391–399. doi:10.1038/nature11405
- 708 Hay M, Thomas DW, Craighead JL, Economides C, Rosenthal J. 2014. Clinical development success rates
709 for investigational drugs. *Nature Biotechnology* **32**:40–51. doi:10.1038/nbt.2786
- 710 Hedrich HJ, Mossman H, Nicklas W. 2004. Chapter 24: Housing and maintenanceThe Laboratory Mouse.
711 Elsevier Academic Press. pp. 395–408.
- 712 Heukelum S van, Mars RB, Guthrie M, Buitelaar JK, Beckmann CF, Tiesinga PHE, Vogt BA, Glennon
713 JC, Havenith MN. 2020. Where is Cingulate Cortex? A Cross-Species View. *Trends in Neurosciences*
714 **43**:285–299. doi:10.1016/j.tins.2020.03.007
- 715 Hodge RD, Bakken TE, Miller JA, Smith KA, Barkan ER, Graybuck LT, Close JL, Long B, Johansen N,
716 Penn O, Yao Z, Eggermont J, Höllt T, Levi BP, Shehata SI, Avermann B, Beller A, Bertagnolli D,
717 Brouner K, Casper T, Cobbs C, Dalley R, Dee N, Ding S-L, Ellenbogen RG, Fong O, Garren E, Goldy
718 J, Gwinn RP, Hirschstein D, Keene CD, Keshk M, Ko AL, Lathia K, Mahfouz A, Maltzer Z, McGraw
719 M, Nguyen TN, Nyhus J, Ojemann JG, Oldre A, Parry S, Reynolds S, Rimorin C, Shapovalova NV,
720 Somasundaram S, Szafer A, Thomsen ER, Tieu M, Quon G, Scheuermann RH, Yuste R, Sunkin SM,
721 Lelieveldt B, Feng D, Ng L, Bernard A, Hawrylycz M, Phillips JW, Tasic B, Zeng H, Jones AR, Koch
722 C, Lein ES. 2019. Conserved cell types with divergent features in human versus mouse cortex. *Nature*
723 **573**:61–68. doi:10.1038/s41586-019-1506-7
- 724 Horev G, Ellegood J, Lerch JP, Son Y-EE, Muthuswamy L, Vogel H, Krieger AM, Buja A, Henkelman RM,
725 Wigler M, Mills AA. 2011. Dosage-dependent phenotypes in models of 16p11.2 lesions found in autism.
726 *Proceedings of the National Academy of Sciences* **108**:17076–17081. doi:10.1073/pnas.1114042108
- 727 Houdebine L-M. 2004. Chapter 6: The mouse as an animal model for human diseasesThe Laboratory Mouse.
728 Elsevier Academic Press. pp. 97–107.
- 729 Kaas JH. 2012. The evolution of neocortex in primates. *Progress in brain research* **195**:91–102.
730 doi:10.1016/B978-0-444-53860-4.00005-2
- 731 Kaas JH. 2011a. Reconstructing the Areal Organization of the Neocortex of the First Mammals. *Brain,*
732 *Behavior and Evolution* **78**:7–21. doi:10.1159/000327316
- 733 Kaas JH. 2011b. Neocortex in early mammals and its subsequent variations. *Annals of the New York*
734 *Academy of Sciences* **1225**:10.1111/j.1749-6632.2011.05981.x. doi:10.1111/j.1749-6632.2011.05981.x
- 735 Krubitzer L. 2007. The Magnificent Compromise: Cortical Field Evolution in Mammals. *Neuron* **56**:201–
736 208. doi:10.1016/j.neuron.2007.10.002
- 737 Laubach M, Amarante LM, Swanson K, White SR. 2018. What, If Anything, Is Rodent Prefrontal Cortex?

- 738 *eneuro* **5**:ENEURO.0315–18.2018. doi:10.1523/ENEURO.0315-18.2018
- 739 Lein ES, Hawrylycz MJ, Ao N, Ayres M, Bensinger A, Bernard A, Boe AF, Boguski MS, Brockway KS,
740 Byrnes EJ, Chen L, Chen L, Chen T-M, Chi Chin M, Chong J, Crook BE, Czaplinska A, Dang CN,
741 Datta S, Dee NR, Desaki AL, Desta T, Diep E, Dolbeare TA, Donelan MJ, Dong H-W, Dougherty JG,
742 Duncan BJ, Ebbert AJ, Eichele G, Estin LK, Faber C, Facer BA, Fields R, Fischer SR, Fliss TP, Frenzley
743 C, Gates SN, Glattfelder KJ, Halverson KR, Hart MR, Hohmann JG, Howell MP, Jeung DP, Johnson
744 RA, Karr PT, Kawal R, Kidney JM, Knapik RH, Kuan CL, Lake JH, Laramee AR, Larsen KD, Lau C,
745 Lemon TA, Liang AJ, Liu Y, Luong LT, Michaels J, Morgan JJ, Morgan RJ, Mortrud MT, Mosqueda
746 NF, Ng LL, Ng R, Orta GJ, Overly CC, Pak TH, Parry SE, Pathak SD, Pearson OC, Puchalski RB,
747 Riley ZL, Rockett HR, Rowland SA, Royall JJ, Ruiz MJ, Sarno NR, Schaffnit K, Shapovalova NV,
748 Sivisay T, Slaughterbeck CR, Smith SC, Smith KA, Smith BI, Sodt AJ, Stewart NN, Stumpf K-R,
749 Sunkin SM, Sutram M, Tam A, Teemer CD, Thaller C, Thompson CL, Varnam LR, Visel A, Whitlock
750 RM, Wohnoutka PE, Wolkey CK, Wong VY, Wood M, Yaylaoglu MB, Young RC, Youngstrom BL, Feng
751 Yuan X, Zhang B, Zwingman TA, Jones AR. 2007. Genome-wide atlas of gene expression in the adult
752 mouse brain. *Nature* **445**:168–176. doi:10.1038/nature05453
- 753 Liu X, Eickhoff SB, Caspers S, Wu J, Genon S, Hoffstaedter F, Mars RB, Sommer IE, Eickhoff CR, Chen
754 J, Jardri R, Reetz K, Dogan I, Aleman A, Kogler L, Gruber O, Caspers J, Mathys C, Patil KR. 2021.
755 Functional parcellation of human and macaque striatum reveals human-specific connectivity in the dorsal
756 caudate. *NeuroImage* **235**:118006. doi:10.1016/j.neuroimage.2021.118006
- 757 Loshchilov I, Hutter F. 2019. Decoupled Weight Decay RegularizationProceedings of the Seventh Interna-
758 tional Conference on Learning Representations. New Orleans.
- 759 Mandino F, Vrooman RM, Foo HE, Yeow LY, Bolton TAW, Salvan P, Teoh CL, Lee CY, Beauchamp A, Luo
760 S, Bi R, Zhang J, Lim GHT, Low N, Sallet J, Gigg J, Lerch JP, Mars RB, Olivo M, Fu Y, Grandjean J.
761 2021. A triple-network organization for the mouse brain. *Molecular Psychiatry* 1–8. doi:10.1038/s41380-
762 021-01298-5
- 763 Markello RD, Arnatkevičiūtė A, Poline J-B, Fulcher BD, Fornito A. 2021. Standardizing workflows in
764 imaging transcriptomics with the abagen toolbox. *Biorxiv* 22.
- 765 Mars RB, Jbabdi S, Rushworth MFS. 2021. A Common Space Approach to Comparative Neuroscience.
766 *Annual Review of Neuroscience* **44**:69–86. doi:10.1146/annurev-neuro-100220-025942
- 767 Mars Rogier B, Passingham RE, Jbabdi S. 2018a. Connectivity Fingerprints: From Areal Descriptions to
768 Abstract Spaces. *Trends in Cognitive Sciences* **22**:1026–1037. doi:10.1016/j.tics.2018.08.009
- 769 Mars RB, Passingham RE, Neubert F-X, Verhagen L, Sallet J. 2016a. Evolutionary specializations of human
770 association cortexEvolution of Nervous Systems. Academic Press. pp. 185–205.

- 771 Mars RB, Sallet J, Neubert F-X, Rushworth MFS. 2013. Connectivity profiles reveal the relationship between
772 brain areas for social cognition in human and monkey temporoparietal cortex. *Proceedings of the National*
773 *Academy of Sciences* **110**:10806–10811. doi:10.1073/pnas.1302956110
- 774 Mars Rogier B, Sotiropoulos SN, Passingham RE, Sallet J, Verhagen L, Khrapitchev AA, Sibson N, Jbabdi S.
775 2018b. Whole brain comparative anatomy using connectivity blueprints. *eLife* **7**. doi:10.7554/eLife.35237
- 776 Mars RB, Verhagen L, Gladwin TE, Neubert F-X, Sallet J, Rushworth MFS. 2016b. Comparing
777 brains by matching connectivity profiles. *Neuroscience & Biobehavioral Reviews* **60**:90–97.
778 doi:10.1016/j.neubiorev.2015.10.008
- 779 Myers E. 2017. Molecular neuroanatomy: Mouse-human homologies and the landscape of genes implicated
780 in language disorders (PhD thesis). Boston University.
- 781 NCBI. 2018. Database resources of the National Center for Biotechnology Information. *Nucleic Acids*
782 *Research* **46**:D8–D13. doi:10.1093/nar/gkx1095
- 783 Neubert F-X, Mars RB, Thomas AG, Sallet J, Rushworth MFS. 2014. Comparison of Human Ventral
784 Frontal Cortex Areas for Cognitive Control and Language with Areas in Monkey Frontal Cortex. *Neuron*
785 **81**:700–713. doi:10.1016/j.neuron.2013.11.012
- 786 Oh SW, Harris JA, Ng L, Winslow B, Cain N, Mihalas S, Wang Q, Lau C, Kuan L, Henry AM, Mortrud MT,
787 Ouellette B, Nguyen TN, Sorensen SA, Slaughterbeck CR, Wakeman W, Li Y, Feng D, Ho A, Nicholas
788 E, Hirokawa KE, Bohn P, Joines KM, Peng H, Hawrylycz MJ, Phillips JW, Hohmann JG, Wohnoutka
789 P, Gerfen CR, Koch C, Bernard A, Dang C, Jones AR, Zeng H. 2014. A mesoscale connectome of the
790 mouse brain. *Nature* **508**:207–214. doi:10.1038/nature13186
- 791 Ortiz C, Fernandez Navarro J, Jurek A, Martin A, Lundeberg J, Meletis K. 2020. Molecular atlas of the
792 adult mouse brain. *Science Advances* **6**:14.
- 793 Pagani M, Barsotti N, Bertero A, Trakoshis S, Ulysse L, Locarno A, Miseviciute I, De Felice A, Canella C,
794 Supekar K, Galbusera A, Menon V, Tonini R, Deco G, Lombardo MV, Pasqualetti M, Gozzi A. 2021.
795 mTOR-related synaptic pathology causes autism spectrum disorder-associated functional hyperconnec-
796 tivity. *Nature Communications* **12**:6084. doi:10.1038/s41467-021-26131-z
- 797 Passingham RE, Stephan KE, Kotter R. 2002. The anatomical basis of functional localization in the cortex.
798 *Nature Reviews Neuroscience* **3**:606–616. doi:10.1038/nrn893
- 799 Preuss TM. 1995. Do rats have prefrontal cortex? The Rose-Woolsey-Akert program reconsidered. *Journal*
800 *of Cognitive Neuroscience* **7**:24.
- 801 Qiu LR, Fernandes DJ, Szulc-Lerch KU, Dazai J, Nieman BJ, Turnbull DH, Foster JA, Palmert MR, Lerch
802 JP. 2018. Mouse MRI shows brain areas relatively larger in males emerge before those larger in females.
803 *Nature Communications* **9**:2615. doi:10.1038/s41467-018-04921-2

- 804 Richards K, Watson C, Buckley RF, Kurniawan ND, Yang Z, Keller MD, Beare R, Bartlett PF, Egan
805 GF, Galloway GJ, Paxinos G, Petrou S, Reutens DC. 2011. Segmentation of the mouse hippocampal
806 formation in magnetic resonance images. *NeuroImage* **58**:732–740. doi:10.1016/j.neuroimage.2011.06.025
- 807 Rudebeck PH, Izquierdo A. 2022. Foraging with the frontal cortex: A cross-species evaluation of reward-
808 guided behavior. *Neuropsychopharmacology* **47**:134–146. doi:10.1038/s41386-021-01140-0
- 809 Sallet J, Mars RB, Noonan MP, Neubert F-X, Jbabdi S, O'Reilly JX, Filippini N, Thomas AG, Rushworth
810 MF. 2013. The Organization of Dorsal Frontal Cortex in Humans and Macaques. *Journal of Neuroscience*
811 **33**:12255–12274. doi:10.1523/JNEUROSCI.5108-12.2013
- 812 Schaeffer DJ, Hori Y, Gilbert KM, Gati JS, Menon RS, Everling S. 2020. Divergence of rodent and pri-
813 mate medial frontal cortex functional connectivity. *Proceedings of the National Academy of Sciences*
814 **117**:21681–21689. doi:10.1073/pnas.2003181117
- 815 Simonoff E, Pickles A, Charman T, Chandler S, Loucas T, Baird G. 2008. Psychiatric Disorders in Children
816 With Autism Spectrum Disorders: Prevalence, Comorbidity, and Associated Factors in a Population-
817 Derived Sample. *Journal of the American Academy of Child & Adolescent Psychiatry* **47**:921–929.
818 doi:10.1097/CHI.0b013e318179964f
- 819 Stahl PL, Salmén F, Vickovic S, Lundmark A, Navarro JF, Magnusson J, Giacomello S, Asp M, Westholm
820 JO, Huss M, Mollbrink A, Linnarsson S, Codeluppi S, Borg Å, Pontén F, Costea PI, Sahlén P, Mulder
821 J, Bergmann O, Lundeberg J, Frisén J. 2016. Visualization and analysis of gene expression in tissue
822 sections by spatial transcriptomics. *Science* **353**:78–82. doi:10.1126/science.aaf2403
- 823 Steadman PE, Ellegood J, Szulc KU, Turnbull DH, Joyner AL, Henkelman RM, Lerch JP. 2014. Genetic
824 Effects on Cerebellar Structure Across Mouse Models of Autism Using a Magnetic Resonance Imaging
825 Atlas: MRI of genetic mouse model's cerebellum. *Autism Research* **7**:124–137. doi:10.1002/aur.1344
- 826 Striedter GF, Northcutt RG. 2020. Brains Through Time. Oxford University Press.
- 827 Sundararajan M, Taly A, Yan Q. 2017. Axiomatic Attribution for Deep NetworksProceedings of the 34th
828 International Conference on Machine Learning. PMLR. pp. 3319–3328.
- 829 Ullmann JFP, Watson C, Janke AL, Kurniawan ND, Reutens DC. 2013. A segmentation protocol and MRI
830 atlas of the C57BL/6J mouse neocortex. *NeuroImage* **78**:196–203. doi:10.1016/j.neuroimage.2013.04.008
- 831 Ventura-Antunes L, Mota B, Herculano-Houzel S. 2013. Different scaling of white matter volume, cor-
832 tical connectivity, and gyration across rodent and primate brains. *Frontiers in Neuroanatomy* **7**.
833 doi:10.3389/fnana.2013.00003
- 834 Vickovic S, Eraslan G, Salmén F, Klughammer J, Stenbeck L, Schapiro D, Äijö T, Bonneau R, Bergenstråhlé
835 L, Navarro JF, Gould J, Griffin GK, Borg Å, Ronaghi M, Frisén J, Lundeberg J, Regev A, Ståhl PL.
836 2019. High-definition spatial transcriptomics for in situ tissue profiling. *Nature methods* **16**:987–990.

837 doi:10.1038/s41592-019-0548-y

- 838 Wang Q, Ding S-L, Li Y, Royall J, Feng D, Lesnar P, Graddis N, Naeemi M, Facer B, Ho A, Dolbeare T,
839 Blanchard B, Dee N, Wakeman W, Hirokawa KE, Szafer A, Sunkin SM, Oh SW, Bernard A, Phillips
840 JW, Hawrylycz M, Koch C, Zeng H, Harris JA, Ng L. 2020. The Allen Mouse Brain Common Coordinate
841 Framework: A 3D Reference Atlas. *Cell* **181**:936–953.e20. doi:10.1016/j.cell.2020.04.007
- 842 Yao Z, Velthoven CTJ van, Nguyen TN, Goldy J, Sedeno-Cortes AE, Baftizadeh F, Bertagnoli D, Casper
843 T, Chiang M, Crichton K, Ding S-L, Fong O, Garren E, Glandon A, Gouwens NW, Gray J, Graybuck
844 LT, Hawrylycz MJ, Hirschstein D, Kroll M, Lathia K, Lee C, Levi B, McMillen D, Mok S, Pham T,
845 Ren Q, Rimorin C, Shapovalova N, Sulc J, Sunkin SM, Tieu M, Torkelson A, Tung H, Ward K, Dee N,
846 Smith KA, Tasic B, Zeng H. 2021. A taxonomy of transcriptomic cell types across the isocortex and
847 hippocampal formation. *Cell* **184**:3222–3241.e26. doi:10.1016/j.cell.2021.04.021

848 **Figure supplements**

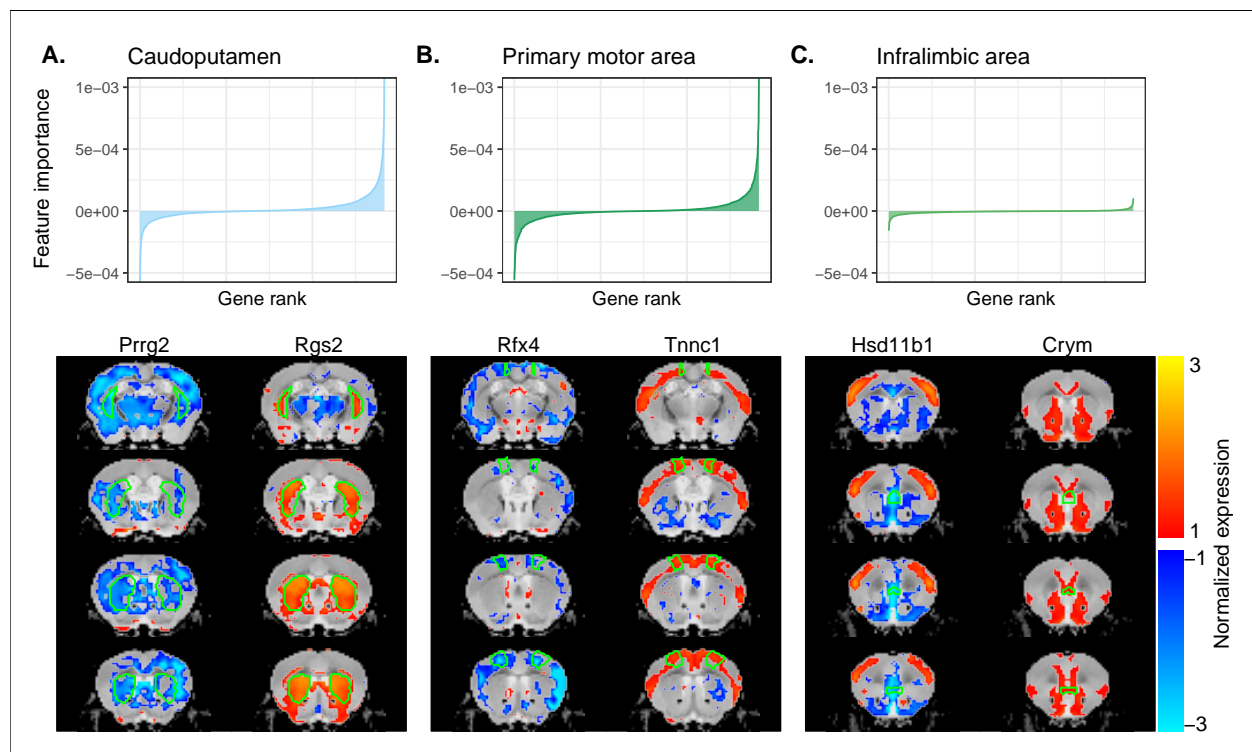


Figure 2-figure supplement 1. Multi-layer perceptron feature importance.